Basin Research

WILEY

Basin Research IAS EAGE

RESEARCH ARTICLE OPEN ACCESS

Buried Pockmarks Associated With Listric Faults of Salt Minibasins (Espírito Santo, SE Brazil): Evidence for Local Hydrocarbon Escape Since the Miocene

Qiang Zhang[1,2,3] | Tiago M. Alves[3] | Marco Antonio Caçador Martins-Ferreira[4]

[1]State Key Laboratory of Deep Oil and Gas, China University of Petroleum (East China), Qingdao, People's Republic of China | [2]School of Geosciences, China University of Petroleum (East China), Qingdao, People's Republic of China | [3]3D Seismic Lab, School of Earth and Environmental Sciences, Cardiff University, Cardiff, UK | [4]Universidade de Brasília, Instituto de Geociências, Campus Universitário Darcy Ribeiro, Brasília, Brazil

Correspondence: Tiago M. Alves (alvest@cardiff.ac.uk)

Received: 26 November 2023 | **Revised:** 24 December 2024 | **Accepted:** 27 December 2024

Funding: This work was supported by China Scholarship Council.

Keywords: buried pockmarks | fluid escape | listric faults | salt minibasin | SE Brazil

ABSTRACT

Buried pockmarks are features associated with fluid seepage through ancient seafloors. In this work, high-quality 3D seismic reflection and well data are used to investigate the geometry, distribution and significance of listric faults and associated pockmarks in a salt minibasin from offshore Espírito Santo, SE Brazil. The results show that six out of ten pockmarks interpreted in the study area have crescent, elliptical, or elongated shapes. They occur along the trace of listric faults and on their immediate hanging-wall blocks, with pockmarks' long axes being nearly parallel to the strike of the faults. The pockmarks are approximately 1300–6200 m long, 600–4000 m wide, 30–139 m deep, and buried 50 to 500 m below the modern seafloor. They can be divided into fault-strike (type I) and fault hanging-wall (type II) pockmarks based on their spatial relationships. Type I represents pockmarks developed along the trace of listric faults, which acted as fluid conduits. Type II pockmarks were developed away from fault traces on their hanging-wall blocks. Their occurrence near listric faults was controlled by multiple factors, including the relative depth, length, area, and maximum displacement of listric faults. In addition, listric faults below horizon H4—an Upper Paleogene unconformity—do not show pockmarks around them. Listric faults with greater length, area, and maximum displacements were more likely to form pockmarks. In conclusion, the studied pockmarks are evidence for local hydrocarbon escape occurring in the Espírito Santo Basin since the Miocene. The results presented here can be applied to other regions around the world prone to geohazards and where carbon and hydrogen storage solutions are being proposed.

1 | Introduction

Pockmarks are seafloor depressions considered as unequivocal indicators of fluid seepage (King and Maclean 1970; Hovland and Judd 1988). They were first reported by King and Maclean (1970) after they found small 'blips' on echosounder profiles from the Scotian Shelf, Canada. Since then, pockmarks have been documented in regions such as the North Sea (Hovland and Sommerville 1985; Cole, Stewart, and Cartwright 2000), Gulf of Mexico (MacDonald et al. 1990; Roelofse, Alves, and Gafeira 2020), Gulf of Cadiz (Ercilla 1996; Maestro et al. 2002; León et al. 2010), West Africa (Ondréas et al. 2005; Gay and Berndt 2007; Pilcher and Argent 2007), and South China Sea (Sun et al. 2011, 2012, 2013; Chen et al. 2015). Seabed pockmarks have been systematically studied due to their relevance to hydrocarbon exploration and production (Hovland and Sommerville 1985; Heggland 1998; Andresen et al. 2011). They are also known to impact the bio-, hydro- and atmosphere

Summary

- Crescent, elliptical and elongated pockmarks are near-parallel to listric faults.
- Pockmarks are controlled by the geometry and attributes of listric faults.
- Differing fluid escape processes relate to two types of pockmarks.
- The studied pockmarks are evidence for fluid escape occurring since the Miocene.

(Hovland and Judd 1988; Hovland et al. 2005; Gay, Lopez, Ondreas, et al. 2006; Judd and Hovland 2007), and are often related to local geohazards (Ligtenberg and Connolly 2003; Judd et al. 2007; Pilcher and Argent 2007; Cathles, Su, and Chen 2010).

Pockmarks usually occur as seafloor depressions with diameters between 10 and 700 m and depths between 1 and 45 m (Hovland, Gardner, and Judd 2002) (Figure 1). The largest pockmarks can reach diameters of > 1 km, to a maximum of 5 km and a depth of up to 200 m (Cole, Stewart, and Cartwright 2000; Davy et al. 2010; Marcon et al. 2014). They can be elongated, crescent, asymmetric, or irregular in shape, and even organised to form composite patterns such as pockmark strings, composite pockmarks, and pockmark groups (Hovland, Gardner, and Judd 2002; Pilcher and Argent 2007; Chen et al. 2015) (Figure 1). Differing shapes or patterns in pockmarks are likely associated with the presence of coalescing clusters, underlying faults, bottom currents, or authigenic carbonates (Pilcher and Argent 2007; Andresen, Huuse, and Clausen 2008; Geldof et al. 2014; Chen et al. 2015). Based on their diameter, pockmarks are subdivided into unit pockmarks (typically < 10 m in diameter), normal pockmarks (tens of meters in diameter), giant pockmarks (hundreds of meters in diameter), and mega pockmarks with diameters of several kilometres (Hovland, Gardner, and Judd 2002; Ondréas et al. 2005; Gay, Lopez, Ondreas, et al. 2006; Pilcher and Argent 2007; Sun et al. 2011; Chen et al. 2015).

In terms of their internal shape, pockmarks can be conical to flat-bottomed, with internal slopes ranging from 6° to 25° (Fader 1991; Pilcher and Argent 2007; León et al. 2010). Their differing V- and U-shapes in cross section also reflect different stages of pockmark development (Masoumi et al. 2014) (Figure 1). Typically, V-shaped pockmarks are formed in the initial stages of fluid seepage from a point source and can later develop into U-shaped pockmarks via slumping, current scouring or draping by hemipelagic sediment (Dimitrov and Dontcheva 1994; Betzler et al. 2011; Masoumi et al. 2014; Roelofse 2020). Large pockmarks can also be active for relatively long periods of time, a phenomenon better confirmed in seismic reflection data (Gay, Lopez, Ondreas, et al. 2006; Roelofse, Alves, and Gafeira 2020; Cao, Sun, and Magee 2023). Conversely, pockmarks buried by recent sediment indicate their activity has ceased and have become palaeo-pockmarks through which only older fluid seepage has occurred (Cole, Stewart, and Cartwright 2000; Gay, Lopez, Ondreas, et al. 2006; Andresen et al. 2011; Hartwig, Anka, and di Primio 2012).

Pockmarks occur either in isolation or form patches with random spatial distributions (Judd and Hovland 2007; Cathles, Su, and Chen 2010; Hovland et al. 2010). Importantly, fluid forming pockmarks can vary from oil, thermogenic and biogenic gas (methane), to pore water (brine) and even fresh water (Hovland and Sommerville 1985; Hovland and Judd 1988; Gay, Lopez, Cochonat, et al. 2006; Judd and Hovland 2007; Andresen, Huuse, and Clausen 2008). The traditional conceptual model proposed by Hovland and Judd (1988) illustrates their formation process as starting via an increase in sediment pore pressure near the seafloor due to the accumulation of gas. This process triggers the generation of small domes over which small tension fractures are formed. In a second stage, gas migrates towards the seafloor through these tension fractures and expands when rising due to a drop in confining pressure (Hovland and Judd 1988). Such a gas expansion results in the fluidisation of surrounding sediment, which is then entrained by the gas to form a mixed gas-sediment plume that ascends into the water column, thereby producing a pockmark on the seafloor (Judd and Hovland 2007, P192-193). An alternative model has been suggested by Cathles, Su, and Chen (2010); in such a model, capillary invasion is preferred as a key process and gas trapped at a capillary seal accumulates to a critical column height. When this column exceeds a threshold value, the buoyancy at the top of seal forces gas through the pore throats. The seal then fails completely, releasing the fluid accumulated below the seal as an upward-propagating gas chimney. Near seafloor sediments are suspended by the upward flow and removed by ocean bottom currents, resulting in the formation of a pockmark (Cathles, Su, and Chen 2010).

Pockmarks can appear spatially organised, with their formation relating to buried geological features such as faults, palaeochannels, palaeocanyons, and diapirs or, instead, to the local remobilisation of seafloor sediment (Cartwright, Huuse, and Aplin 2007; Gay et al. 2007; Judd and Hovland 2007; Pilcher and Argent 2007; de Mahiques et al. 2017; Velayatham, Holford, and Bunch 2018). In fact, phenomena that reduce local lithostatic pressure are capable of initiating and localising pockmarks in nature (Gay et al. 2007; Pilcher and Argent 2007). The presence of faults usually plays an important role in pockmark formation (e.g., Hovland and Judd 1988; Soter 1999; Sun et al. 2011; Chen et al. 2015; Velayatham, Holford, and Bunch 2018). For instance, Soter (1999) used sidescan sonar data to report a pockmark chain along the trace of the Aigion Fault (Greece). In the Ebro Delta, NE Spain, Maestro et al. (2002) observed large pockmarks on the hanging-walls of listric faults, and also overlying their footwall cutoffs, to infer that the seeping fluid was biogenic gas produced from organic-rich units. Geochemical analyses of sediment samples from the Lower Congo Basin allowed Gay, Lopez, Cochonat, et al. (2006) to document pockmarks seeping thermogenic gas and oil. They suggested the Lower Congo pockmarks to be associated with fluid migration along vertically stacked turbidite channels and polygonally faulted intervals (Gay, Lopez, Cochonat, et al. 2006). In parallel, Pilcher and Argent (2007) described spatially organised pockmarks

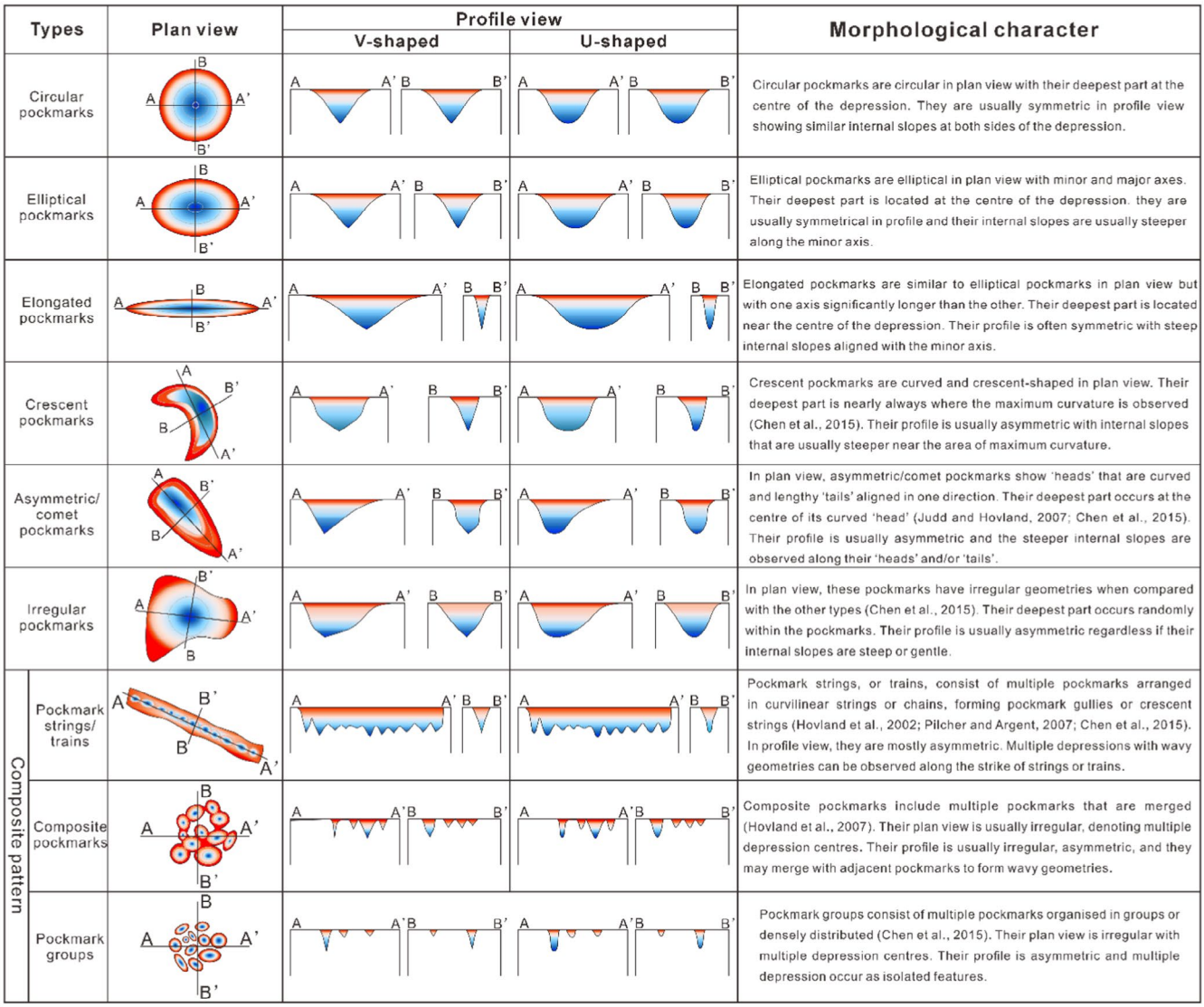

FIGURE 1 | Diagram summarising the geometry of different pockmark types in plan and profile view. Pockmarks with V- and U-shapes in profile view are plotted separately. The classification of different pockmark types is based on Hovland, Gardner, and Judd (2002), Pilcher and Argent (2007) and Chen et al. (2015).

near faults on the West African continental margin and classified them based on the spatial relationships observed. Finally, Velayatham, Holford, and Bunch (2018) studied three linear pockmark trains in the Northern Carnarvon Basin, Australia, the largest being over 72 km long and parallel to an array of linked normal faults. This character led them to suggest that faults act as spatial controls for fluid migration.

Pockmarks have been first investigated in the Espírito Santo Basin by Tao and Alves (2021), who classified them as random and non-random. They interpreted random pockmarks as being formed due to the rapid burial of continental slope strata, while non-random pockmarks relate to the presence of underlying strata-bound domino-style faults. Later, Tao and Alves (2023) described two dissolution pockmarks over salt structures in the Espírito Santo Basin, relating their presence to localised (dissolution-related) upward migration of salt-saturated fluid. Still in the Espírito Santo Basin, Zhang, Alves, and Martins-Ferreira (2022) recorded large pockmarks near the upper part of listric faults, demonstrating the importance of fluid flow along these structures. Notwithstanding such work, detailed quantifications of the relationship between pockmarks and adjacent listric faults are scarce in the Espírito Santo Basin, and also in the published literature, imposing limitations to our understanding of how pockmarks are formed in the submarine environment. Thus, the aim of this work is to investigate the geometry, distribution and significance of buried pockmarks, analysing their relationship to the listric faults from which they stem. In summary, this paper addresses the following research questions:

a. What is the potential relationship between buried pockmarks and adjacent listric faults?

b. How did buried pockmarks form in the investigated salt minibasin from SE Brazil?

c. What is their importance to seal-competence analyses when found in salt minibasins across the world?

2 | Geological Setting

The Espírito Santo Basin is located on the continental margin of SE Brazil and covers an area of ~125,000 km^2, of which 107,000 km^2 are located offshore (Fiduk et al. 2004; Gamboa et al. 2010). The basin is bounded to the north by the Abrolhos Plateau, a volcanic ridge separating the Espírito Santo Basin from the Cumuruxatiba Basin (Figure 2). To the south, it is separated from the Campos Basin by a largely political boundary as there is effectively a continuum of rift, sub-salt, and supra-salt units in SE Brazil when one moves from the Santos to the Espírito Santo basins (Figure 2b; Fiduk et al. 2004; Gamboa et al. 2010; Alves 2012; Mattos and Alves 2018).

The Espírito Santo Basin includes a series of basins trending N–S to NNE–SSW that were formed during Late Jurassic-Early Cretaceous rifting and subsequent continental breakup of the supercontinent Gondwana (Ojeda 1982; Chang et al. 1992; Fiduk et al. 2004; Mohriak, Nemčok, and Enciso 2008; Alves 2012; Piedade and Alves 2017). In fact, the tectonic evolution of the Espírito Santo Basin is similar to most rift basins in the South Atlantic Ocean. Its evolution can therefore be divided into four separate stages: rift onset, syn-rift, transitional, and drift (Chang et al. 1992; Bruhn and Walker 1997; Cobbold, Meisling, and Mount 2001; Fiduk et al. 2004; Gamboa, Alves, and Cartwright 2012) (Figure 3).

2.1 | Rift-Related Evolution of the Espírito Santo Basin

Continental rifting occurred in the Espírito Santo Basin in the Late Jurassic and Early Cretaceous (Ojeda 1982; Cainelli and Mohriak 1999; Fiduk et al. 2004; Mohriak, Nemčok, and Enciso 2008). Moderate tectonism and intense volcanism were recorded throughout SE Brazil during this first rift-onset stage, and the Espírito Santo Basin was rapidly filled with coarse-grained fluvial sediments, alluvial fan deposits and localised evaporites (Ojeda 1982; Chang et al. 1992; Cainelli and Mohriak 1999; Mohriak and Rosendahl 2003).

The syn-rift stage lasted from late Berriasian/Valanginian (earliest Cretaceous) to the early Aptian (Ojeda 1982; Fiduk et al. 2004; Gamboa 2011; Qin et al. 2016). It was marked by intense tectonism due to the enhanced lithospheric extension and asthenospheric uplift that accompanied the formation of the Eastern Brazilian Rift (Cainelli and Mohriak 1999; Mohriak and Rosendahl 2003). Resultant syn-rift units comprise lacustrine sediments deposited in elongated and faulted sub-basins formed between the Santos and the Sergipe/Alagoas Basins. Three main facies associations were deposited at this stage: 1) alluvial fan/fan deltas and transitional deposits, 2) lacustrine marls and shales, and 3) lacustrine pelecypod limestones,

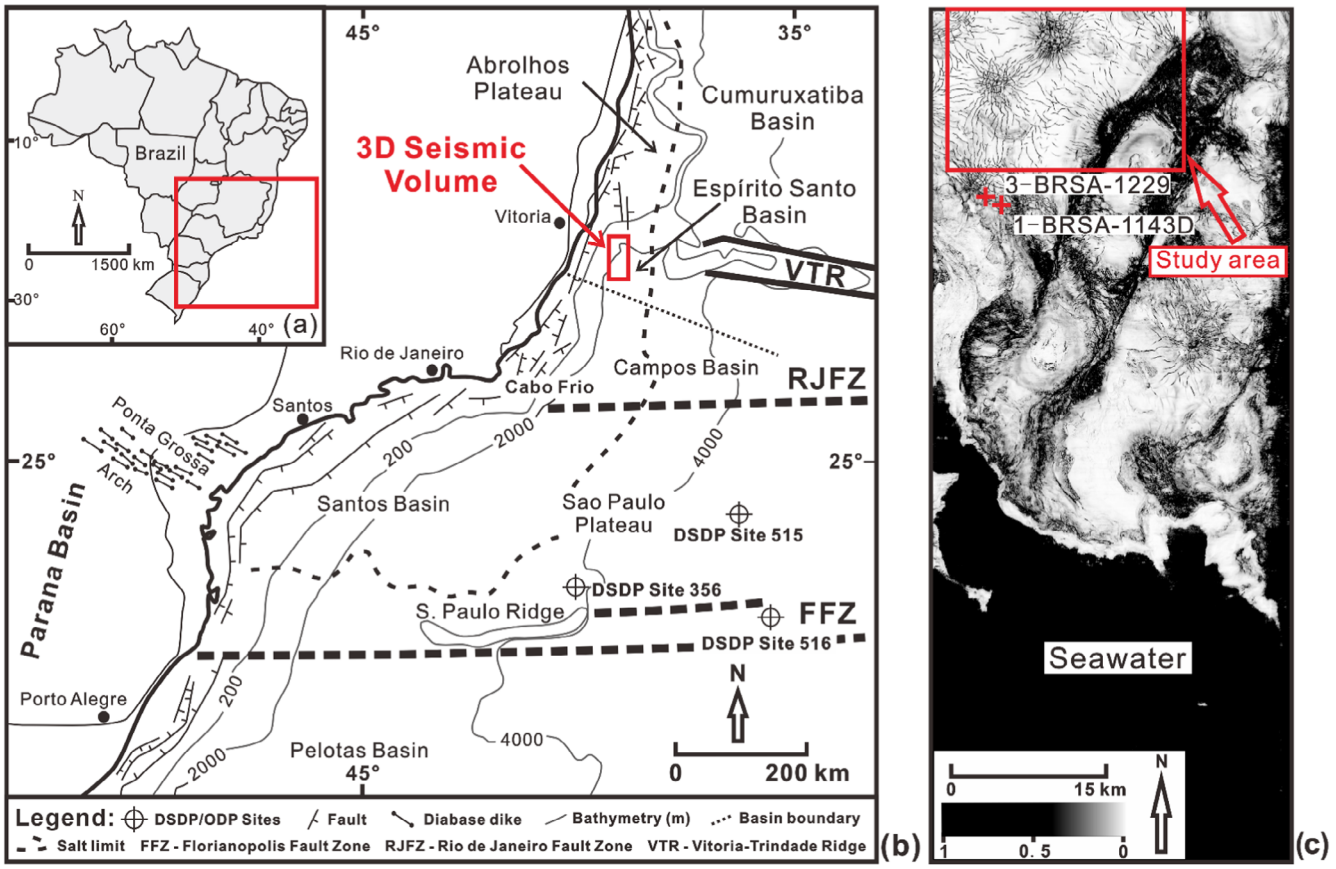

FIGURE 2 | (a) Location of the study area in relation to Brazil and its continental margin. (b) Map highlighting the location of the Espírito Santo Basin and its adjacent structural units. The Espírito Santo Basin is bounded by the volcanic Abrolhos Plateau to the north and is separated from the Campos Basin to the south by a political boundary shown as a black dashed line. The red polygon indicates the location of the 3D seismic volume in (c). (c) Variance time-slice (Z = -3000 ms two-way travel time) of the entire 3D seismic volume showing the location of study area as a red polygon. Two exploration wells (3-BRSA-1229 and 1-BRSA-1143D) are marked as red crosses. (b) modified from Alves (2012).

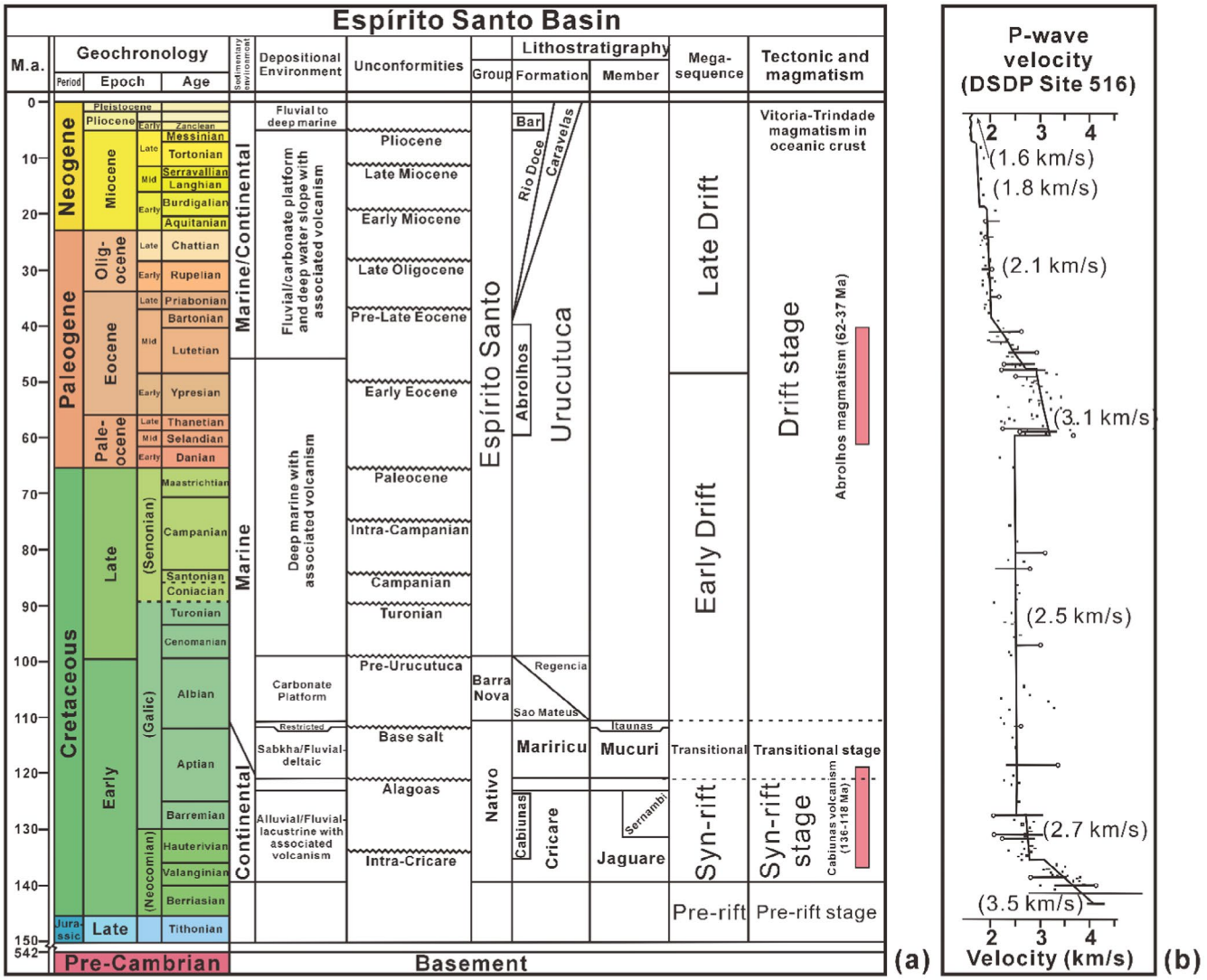

FIGURE 3 | (a) Tectono-stratigraphic chart of the Espírito Santo Basin showing main stratigraphic units and corresponding depositional environments. Four tectonic evolutionary stages, two episodes of magmatism and five megasequences are highlighted in the figure. Figure modified from Mattos and Alves (2018). (b) Velocity data profile for well DSDP 516 for the Rio Grande Rise (Barker, Buffler, and Gambôa 1983). See Figure 2b for the location of DSDP Site 516.

usually termed *coquinas* by the Brazilian geological community (Ojeda 1982; Demercian, Szatmari, and Cobbold 1993; Cainelli and Mohriak 1999) (Figure 4).

2.2 | Basinwide Halokinesis and Its Relationship to SE Brazil's Cenozoic Evolution

The transitional stage occurred from Early Aptian to Late Aptian/Early Albian, a period of time associated with continental breakup occurring to the east (i.e., outboard) of the Espírito Santo Basin (Ojeda 1982; Fiduk et al. 2004; Alves et al. 2020). At this stage, the activity of large faults was concentrated near the loci of continental breakup. Significant lithospheric extension enhanced regional subsidence as recorded by the precipitation and accumulation of >3000 m of evaporites during the Aptian-Early Albian above shallow-water microbial carbonates (Davison, Anderson, and Nuttall 2012) (Figure 4). These transitional strata thus reflect a continental-breakup sequence with a typical regressive-transgressive trend (Alves and Cunha 2018; Alves et al. 2020).

The drift stage occurred from the Albian to present-day and marks the phase of ocean spreading between South America and Africa (Ojeda 1982; Fiduk et al. 2004; Gamboa 2011). Tectonic activity during the drift stage was chiefly associated with thermal subsidence and resulted in widespread deposition of marine strata in the Espírito Santo Basin (Chang et al. 1992; Cainelli and Mohriak 1999). The drift stage comprises two distinct megasequences: early-drift transgressive and late-drift regressive (Chang et al. 1992; Cainelli and Mohriak 1999). The early-drift (transgressive) megasequence records the deposition of carbonate intervals below muddy and sandy turbidites, reflecting shallow-water environments that progressively deepened until the end of the Cretaceous (Ojeda 1982; Chang et al. 1992; Mohriak, Nemčok, and Enciso 2008; Qin et al. 2016) (Figure 4). The late-drift (regressive) megasequence is marked by open marine deposition and

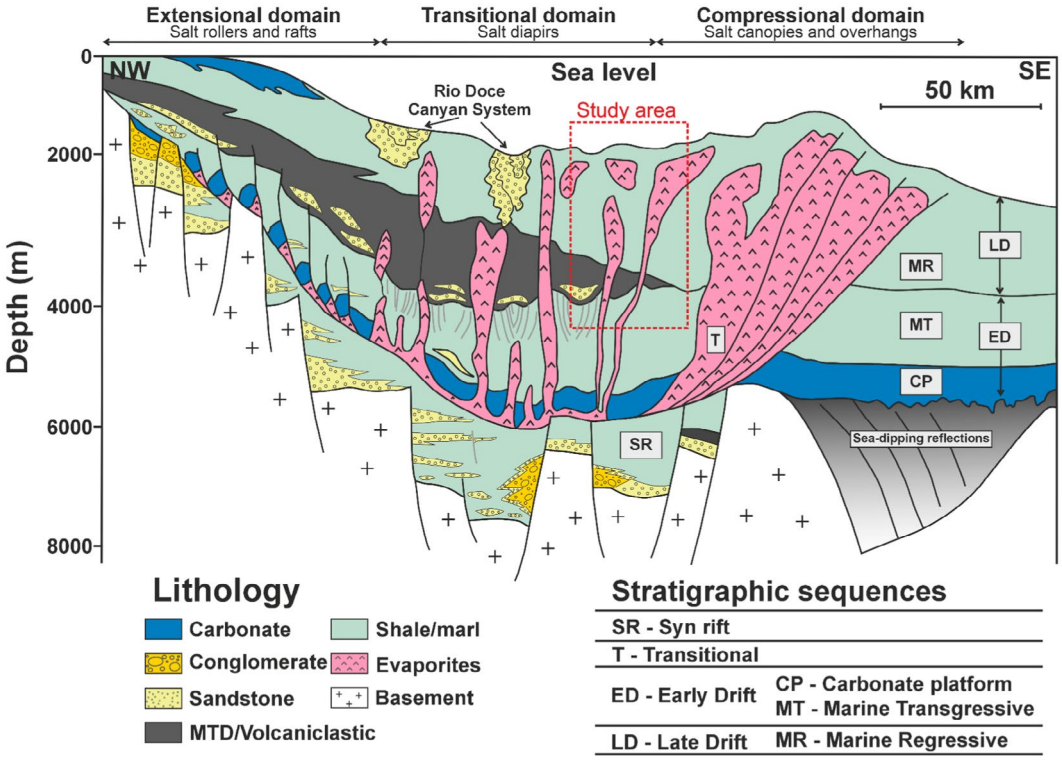

FIGURE 4 | Diagram illustrating the three structural domains of the Espírito Santo Basin and related strata. Tectonic megasequences are also shown. The red polygon indicates the location of study area relative to the three structural domains. Figure modified from Gamboa (2011) and Fiduk et al. (2004).

the progressive filling of the Espírito Santo Basin's continental shelf and slope (Ojeda 1982; Chang et al. 1992; Mohriak, Nemčok, and Enciso 2008) (Figure 4).

Accompanying regional extension and continuous subsidence, halokinesis occurred in the Espírito Santo Basin in response to differential loading by overburden strata, gravity spreading and downslope gravity gliding on top of evaporite successions (Demercian, Szatmari, and Cobbold 1993; Fiduk et al. 2004). Halokinesis lasted from the Albian to Holocene but peaked during the Late Cenozoic (Fiduk et al. 2004; Alves 2012). It also divided the basin into three tectonic domains with different structural styles: proximal extensional, transitional, and distal compressional (Rouby et al. 2003; Vendeville 2005; Gamboa et al. 2010; Mohriak, Szatmari, and Anjos 2012; Qin et al. 2016) (Figure 4). The proximal extensional domain includes salt rollers, salt walls along conjugate normal faults, turtle anticlines and rafts (Mohriak, Nemčok, and Enciso 2008). The transitional domain is characterised by the predominance of salt diapirs, whereas the distal compressional domain is dominated by allochthonous salt (Demercian, Szatmari, and Cobbold 1993; Davison 2007). The study area is situated between the transitional and distal compressional domains of the basin and, consequently, several salt diapirs and a single salt wall are observed in seismic data (Figures 4 and 5).

3 | Data and Methods

This study uses a high-quality 3D seismic volume acquired in deep-water Espírito Santo Basin during 2004, covering 360 km^2 of the SE Brazilian margin (Figure 2c). The seismic volume was shot at a water depth ranging from 1630 to 2050 m. It was acquired with a 6×5700 m array of streamers following a 12.5×12.5 m grid-line spacing. Seismic data processing included resampling, spherical divergence corrections and zero-phase conversions, undertaken prior to data stacking. The seismic data are displayed using European SEG polarity, in which an increase in acoustic impedance is shown as a red seismic reflector. The seismic volume was pre-stacked time migrated following a sampling rate of 2 ms, and re-sampled at 4 ms with a dominant frequency of 40 Hz. This resulted in a minimum vertical resolution (1/4 of the wavelet frequency, or $\lambda/4$) ranging from 11 to 19 m at the depth of the strata investigated in this work as verified by correlating seismic reflection with the available borehole data. Two wells located in vicinity of the study area provided gamma-ray, lithology, V_p (P-wave velocity) and check-shot data (see Biancardi, Alves, and Martins-Ferreira 2020).

The study area comprises a 20 km long, 6 km wide, NE-striking salt minibasin. This minibasin is bounded to the west by salt diapirs A and B, and to the east by a salt wall (Figure 5). Eight key seismic-stratigraphic markers, including the seafloor, were interpreted and tied to known well stratigraphic markers (Figures 7–10). Amongst such markers, horizon H0 correlates with the top of Cretaceous strata in the study area. Paleogene strata above H0 are primarily composed of marl in the lower part and shale in the upper part of the sequence (Figure 5). In seismic data, horizon H0 is expressed as a laterally continuous, parallel reflection of low to moderate amplitude (Figures 8–10). Horizon H5 correlates with the top of Paleogene strata (Figure 5). Above

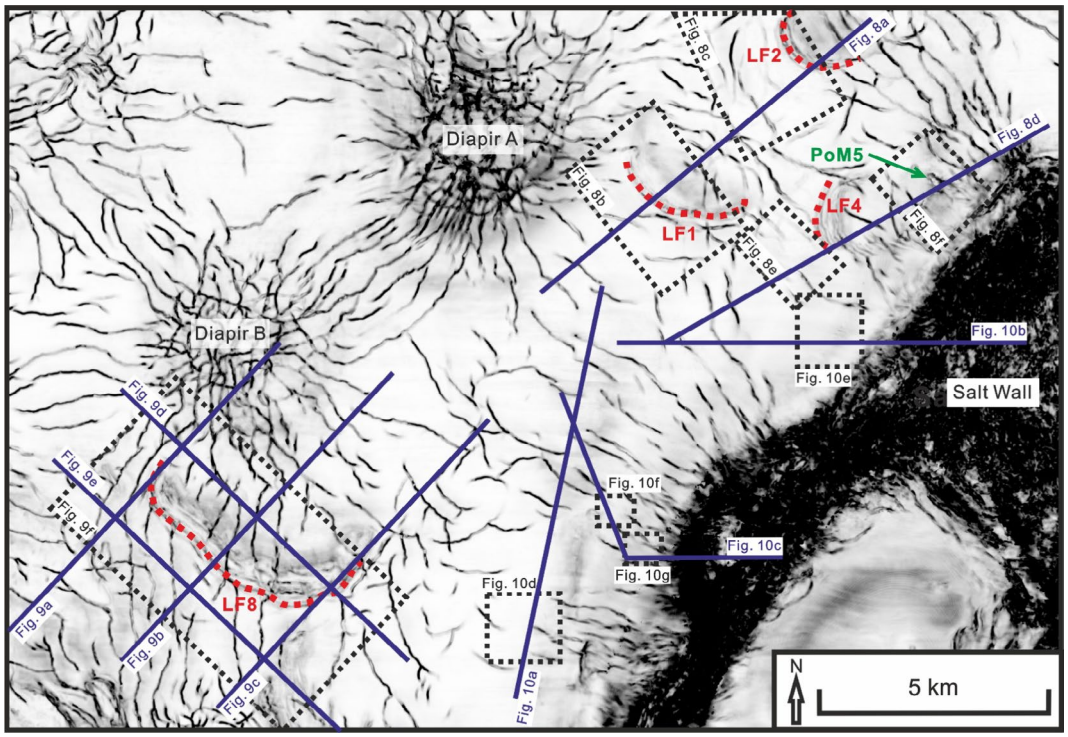

FIGURE 5 | Variance time-slice ($Z = -3000$ ms two-way time) across the study area highlighting the distribution of listric faults, pockmarks and salt structures. Interpreted seismic profiles and the pockmark fields shown in Figures 8–10 are respectively indicated as blue lines and black dashed polygons. LF, Listric fault; PoM, Pockmark.

H5, Miocene strata are essentially clayey. Horizon H5 is a continuous and parallel reflection of high amplitude (Figures 8–10). Between horizons H0 and H5 there are four other stratigraphic boundaries separating particular seismic packages in Paleocene and Eocene strata (Figure 6).

As all investigated pockmarks and listric faults occur within Cenozoic strata, no seismic horizons were interpreted below horizon H0, except for the Top Salt marker. Nevertheless, time-depth conversions were completed for the interpreted seismic survey by using multiple check-shot data provided by the two available boreholes. The Vp data gathered from these two wells reveal an average velocity of 3.0 km/s between horizons H0 and H3, 2.6 km/s between horizons H3 and H6, and 2.0 km/s for the strata occurring between horizon H6 and the seafloor (Figure 6).

Variance time-slices and two-way travel time (TWTT) maps were used to identify buried pockmarks and faults (Figures 5 and 7). Buried pockmarks were identified in the study area and mapped every two crosslines/inlines (25 m) (Figure 7). Detailed 3D structural maps, combined with seismic profiles, revealed the pockmarks' spatial position and distribution (Figures 8–10). The length, width, depth, internal slope, and area of pockmarks were measured to investigate their geometry and relationship with listric faults (Table 1). The internal slope of pockmarks was measured along their short axes and included information on their steep and gentle internal slopes. Hence, pockmark length, width, and depth comprise, in this work, detailed measurements of the pockmarks' long axis length, short axis length and vertical drop from the rim of the depression to their deepest point. The area of pockmarks corresponds to the plan-view size of pockmarks measured in TWTT structural maps.

Ten (10) listric faults were interpreted every two crosslines and inlines (25 m) to guarantee an accurate record of fault attribute data. We measured the strike, dip, length, maximum displacement, throw, heave and area of these 10 listric faults. Fault displacement was calculated using trigonometry rules to determine the throw and heave values for each fault. This was done because listric faults record significant horizontal offsets (heave) when compared to planar, high-angle faults. Measuring throw alone would oversimplify our structural analysis.

Displacement-length (D_{max}-L) and displacement-depth (D-Z) plots were compiled for all listric faults following the criteria of Tao and Alves (2019). The latter authors have shown that the minimum sampling intervals needed for accurate throw/displacement measurements are related to the length of a fault. Hence, sampling intervals should be less than 5% for those faults shorter than 3500 m, and 3% for faults that are 3500 m and longer. It should be noted that the dip and area of listric faults were automatically measured by fault-point data processed on Move. These fault-point data were uploaded on Move by discretising into facets the listric faults that were originally interpreted on Schlumberger's Petrel. Time-depth conversions were implemented on all the faults analysed on Move.

Leakage Factor analyses were completed for the listric faults using Move's Stress Analysis Module and the stress inversion data in Zhang, Alves, and Martins-Ferreira (2022). We assumed that the stress tensors in the area where listric faults occur are, at present, similar to the palaeostress tensors estimated (inverted) by Zhang, Alves, and Martins-Ferreira (2022) for the Late Cenozoic, as there were no significant changes in the tectonic setting of the Espírito Santo Basin since then (Ojeda 1982;

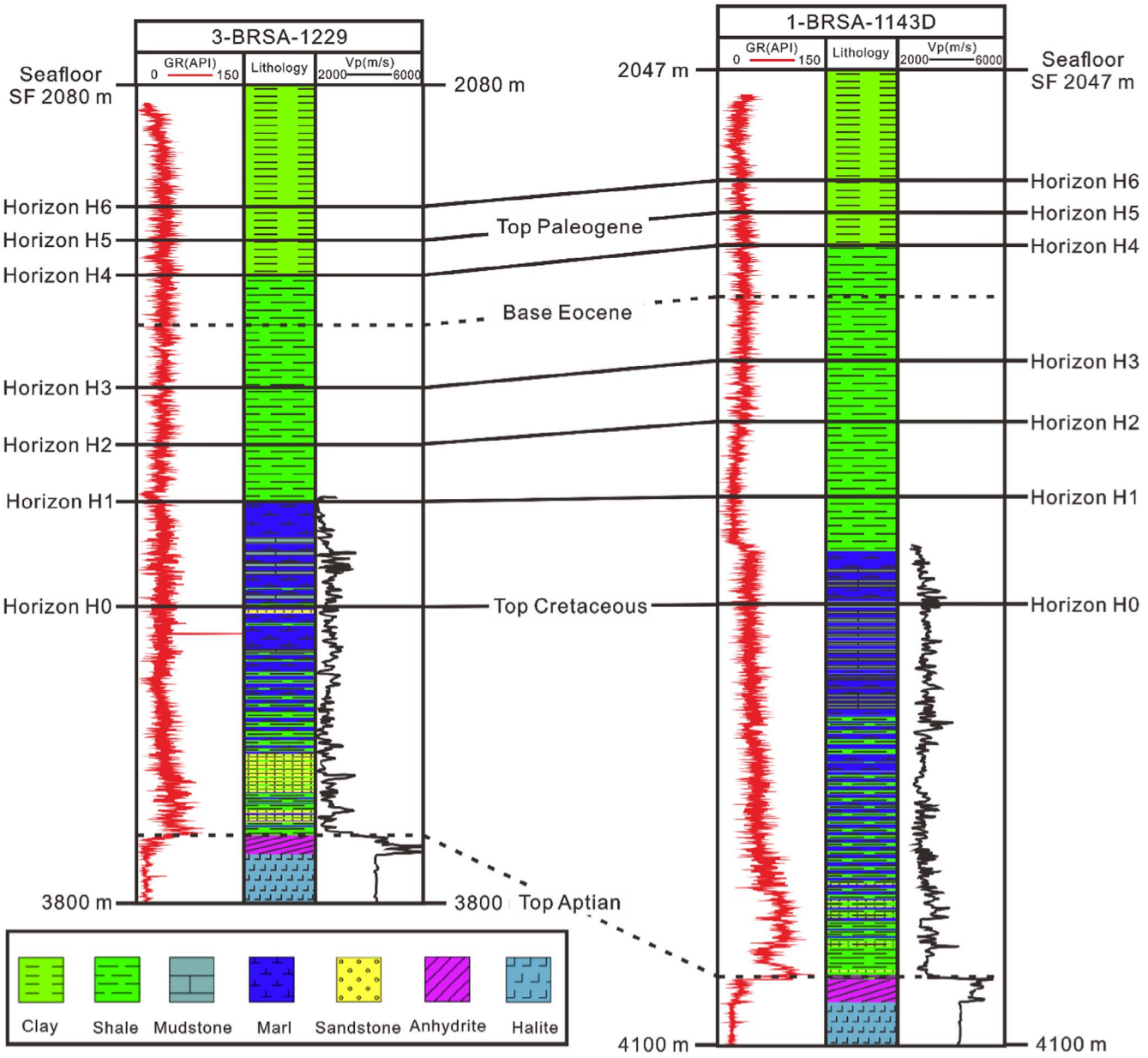

FIGURE 6 | Correlation panel for wells 3-BRSA-1229 and 1-BRSA-1143D drilled near the study area. See location of the two wells in Figure 2c. Chronostratigraphic framework, lithology, gamma-ray (GR) and V_p (P-wave velocity) wireline curves are all shown in the figure.

Fiduk et al. 2004; Gamboa 2011). This assumption is further supported by the fact that the interpreted listric faults have propagated as pure dip-slip faults and almost reach the modern seafloor (Figures 8–10). In addition, Zhang, Alves, and Martins-Ferreira (2022) have shown that listric faults in the study area were formed under a sub-vertical σ_1 plunging −89.4° along an N88.64° azimuth a sub-horizontal σ_2 plunging 0.42° along an N133.64° azimuth and a sub-horizontal σ_3 plunging 0.42° along an N43.63° azimuth. These values were calculated without considering any local stress variations resulting from the rotation of the listric faults.

Fault leakage factors were also calculated using Move, a parameter that considers the ratio of pore pressure (P_p) to the difference between normal (σ_n) and shear stresses (τ) on a particular fault surface. Leakage factor is a measure of the fluid transmissivity in faults and determines the likelihood of fault-seal failure. The higher the leakage factor, the greater is the likelihood of a fault to act as a pathway for fluid. In parallel, the relationship between pockmarks and their adjacent listric faults was analysed by correlating pockmarks' geometry with fault attribute data. Pockmarks were measured along their long axes using the same spacing (25 m) adopted for the fault mapping and for the compilation of faults' D_{max}-L plots.

4 | Results

4.1 | Morphology and Spatial Distribution of Buried Pockmarks

A total of ten (10) buried pockmarks were identified in the study area (Figures 7–10). Six (6) of these pockmarks were developed on the immediate hanging-wall and along the trace of listric

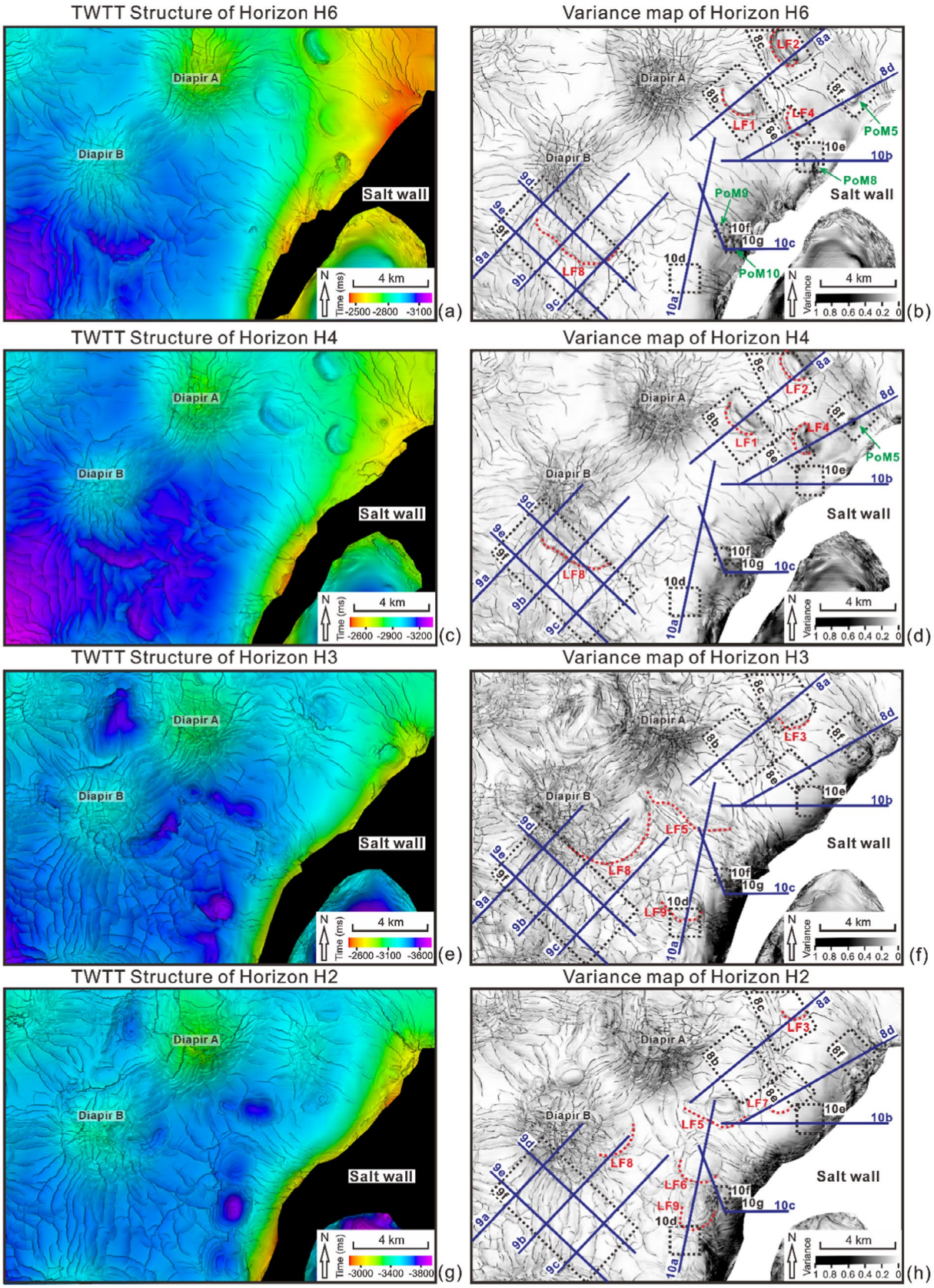

FIGURE 7 | TWTT structural and variance maps for four (4) key seismic-stratigraphic horizons highlighting the spatial distribution of listric faults, pockmarks and salt structures. (a), (c), (e) and (g) TWTT structural maps for horizons H6, H4, H3 and H2. (b), (d), (f) and (h) Variance maps for horizons H6, H4, H3 and H2. Seismic profiles and pockmark positions shown in Figures 8–10 are indicated by blue lines and black dashed polygons, respectively. Horizons H2 and H3 are between the base of Paleocene and Eocene strata, and horizon H6 is between the base of Eocene and Miocene strata. Horizon 6 is above the base of the Miocene strata. LF, Listric fault; PoM, Pockmark.

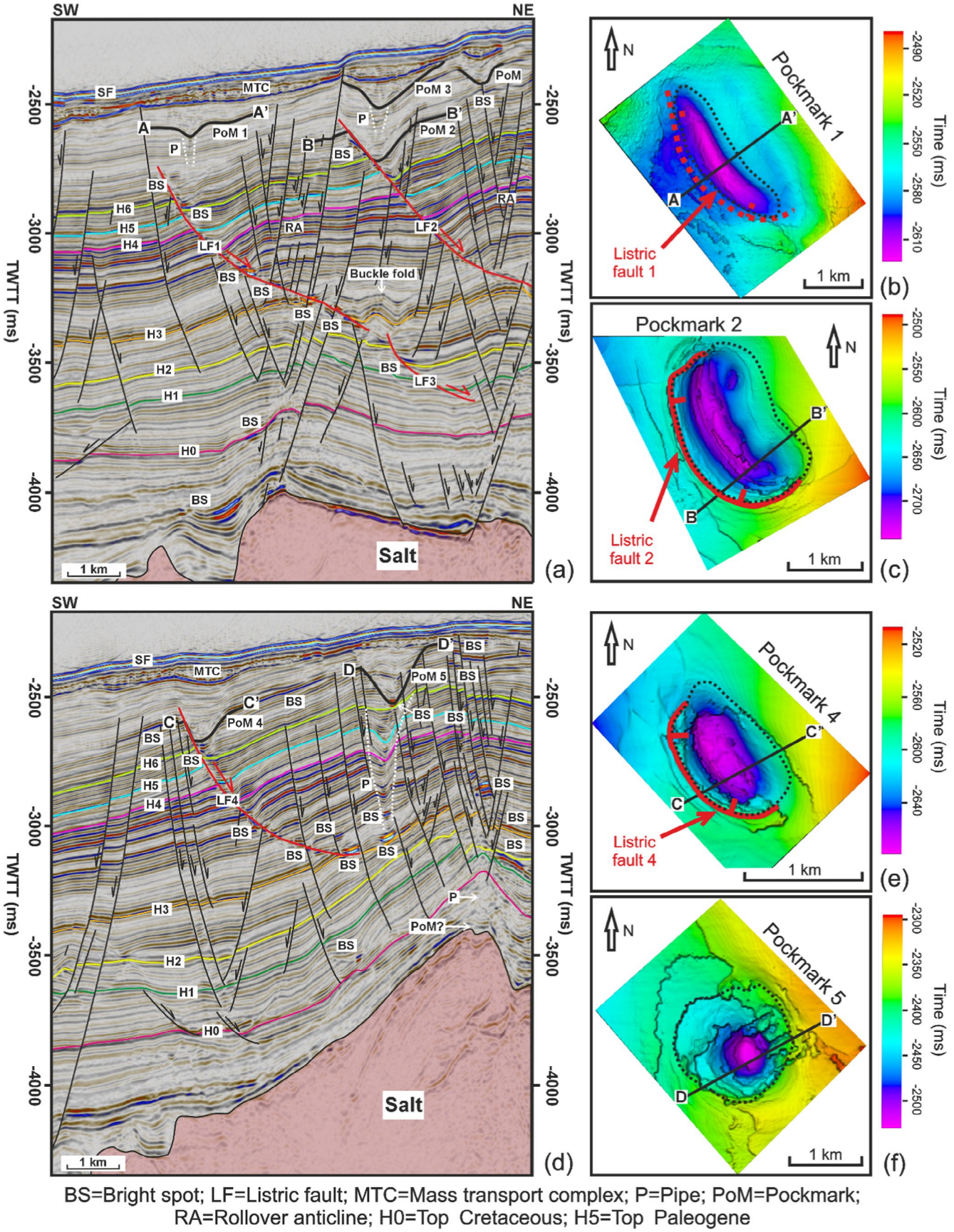

FIGURE 8 | Legend on next page.

FIGURE 8 | Seismic profiles and TWTT structural maps showing the geometry and spatial distribution of pockmarks 1, 2, 4 and 5. (a) and (d) Seismic profiles across some of the pockmarks interpreted in this work. (b), (c), (e) and (f) 3D visualisation of interpreted pockmarks as bounded by black dash polygons and their corresponding listric faults. The black lines shown in (b), (c), (e) and (f) indicate the seismic reflections marked by the labelled bold black lines in (a) and (d). The location of seismic profiles and pockmarks are shown in Figures 5 and 7. See uninterpreted seismic profiles in Supporting Information File S1.

TABLE 1 | Statistical data for the studied pockmarks.

Name	Plan-view shape	Length (m)	Width (m)	Length: width ratio	Depth (m)	Steep internal slope	Gentle internal slope	Area (km^2)	Relative position
Pockmark 1	Elongated	2339	551	4.2	33	7	6	1.2	Along the trace of listric fault 1
Pockmark 2	Crescent	2283	1150	2.0	104	9	7	2.5	Along the trace of listric fault 2
Pockmark 3	Elliptical	1674	1177	1.4	61	6	4	1.9	On the hanging-wall of listric fault 2
Pockmark 4	Elliptical	1288	739	1.7	75	12	11	0.7	Along the trace of listric fault 4
Pockmark 5	Circular	1125	1027	1.1	76	10	8	0.9	On the hanging-wall of crestal fault
Pockmark 6	Elliptical	6238	3986	1.6	94	6	2	15.8	Along the trace of listric fault 8
Pockmark 7	Elliptical	1362	884	1.5	139	20	20	1.1	Along the trace of listric fault 9
Pockmark 8	Circular	1100	1061	1.0	138	9	8	0.9	Along the flank of salt wall
Pockmark 9	Elliptical	485	322	1.5	85	23	17	0.1	Along the flank of salt wall
Pockmark 10	Elliptical	426	228	1.9	23	23	20	0.1	Along the flank of salt wall

Note: Steep and gentle internal slopes were measured along the short axes of pockmarks. The location of the pockmarks is shown in Figures 7–10.

faults (Figures 8–10). The other four (4) pockmarks occur near the crestal faults of salt diapirs and along the flank of the salt wall (Figures 8–10). Based on these observations, we name the former pockmarks as Type I, associated with listric faults, and the latter crestal/salt wall pockmarks as Type II (Figures 7–10).

4.1.1 | Type I Pockmarks

Type I pockmarks are crescent, elliptical or elongated in plan view, 1288 to 6238 m long, 551 to 3986 m wide and 33 to 139 m deep (Figures 8–10; Table 1). Their steep internal slopes vary between 6° and 20°, while their gentle internal slopes are between 2° and 19°. Their plan-view area varies from 0.7 to 15.8 km^2. Type I pockmarks occur above horizon H5—the Top Paleogene unconformity—except for pockmark 7, which occurs between horizons H3 and H4. This character shows Type I pockmarks were formed after the Paleogene (Figures 8–10).

Type I pockmarks are found on the hanging-wall of listric faults or along their traces. In cross section, the pockmarks are U-shaped or tabular, with onlapping infills *sensu* Mitchum Jr., Vail, and Sangree (1977) and Andresen, Huuse, and Clausen (2008). This onlapping sediment has low amplitude, is chaotic in places, and contrasts markedly with the higher amplitude (undeformed) slope strata (Figures 8a,d, 9a–e, and 10a). Sediment filling pockmarks 3 and 6 is locally eroded near the seafloor by a mass transport complex (MTC), resulting in local strata thinning (Figures 8a and 9a–e). This MTC is bounded by a high-amplitude negative reflection at its base, and contains low-amplitude chaotic reflections in its interior (Figures 7–10).

Type I pockmarks have long axes that are parallel to the strike of listric faults, i.e. NW-SE to WNW-ESE (Figures 7–10). Based on the classification proposed by Pilcher and Argent (2007), they are separated into fault-strike and fault hanging-wall pockmarks. Fault-strike pockmarks are developed along the trace of faults,

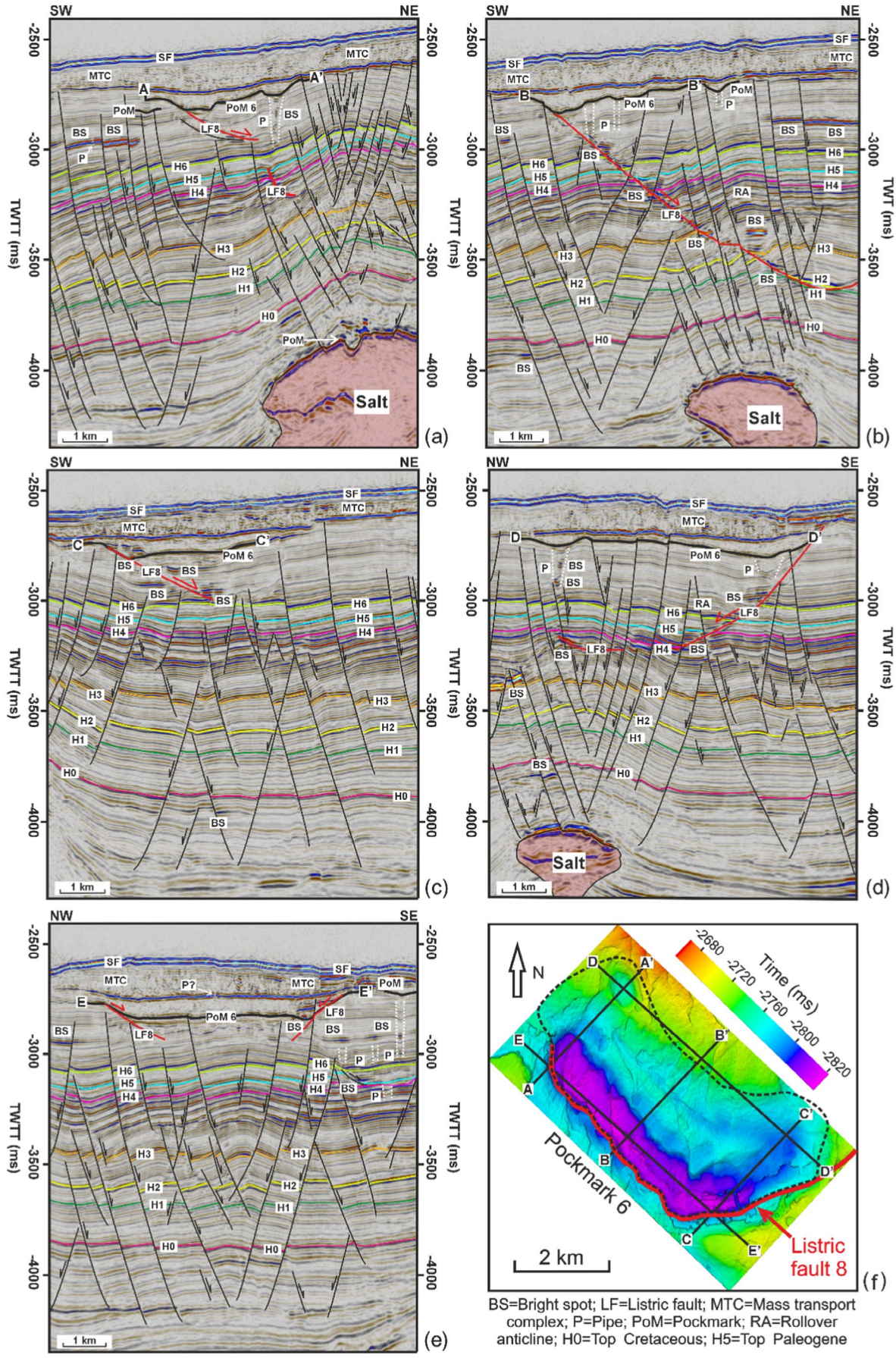

FIGURE 9 | Legend on next page.

FIGURE 9 | Seismic profiles and TWTT structural map highlighting the geometry and spatial distribution of pockmark 6. (a–e) Seismic profiles across pockmark 6. (f) 3D visualisation of pockmark 6, which is bounded in the figure by black dash polygons and listric fault 8. The black lines in (f) indicate the seismic reflection marked by the bold black lines in (a–e). The location of seismic profiles and pockmark 6 is shown in Figures 5 and 7. See also the uninterpreted seismic profiles in Supporting Information File S1.

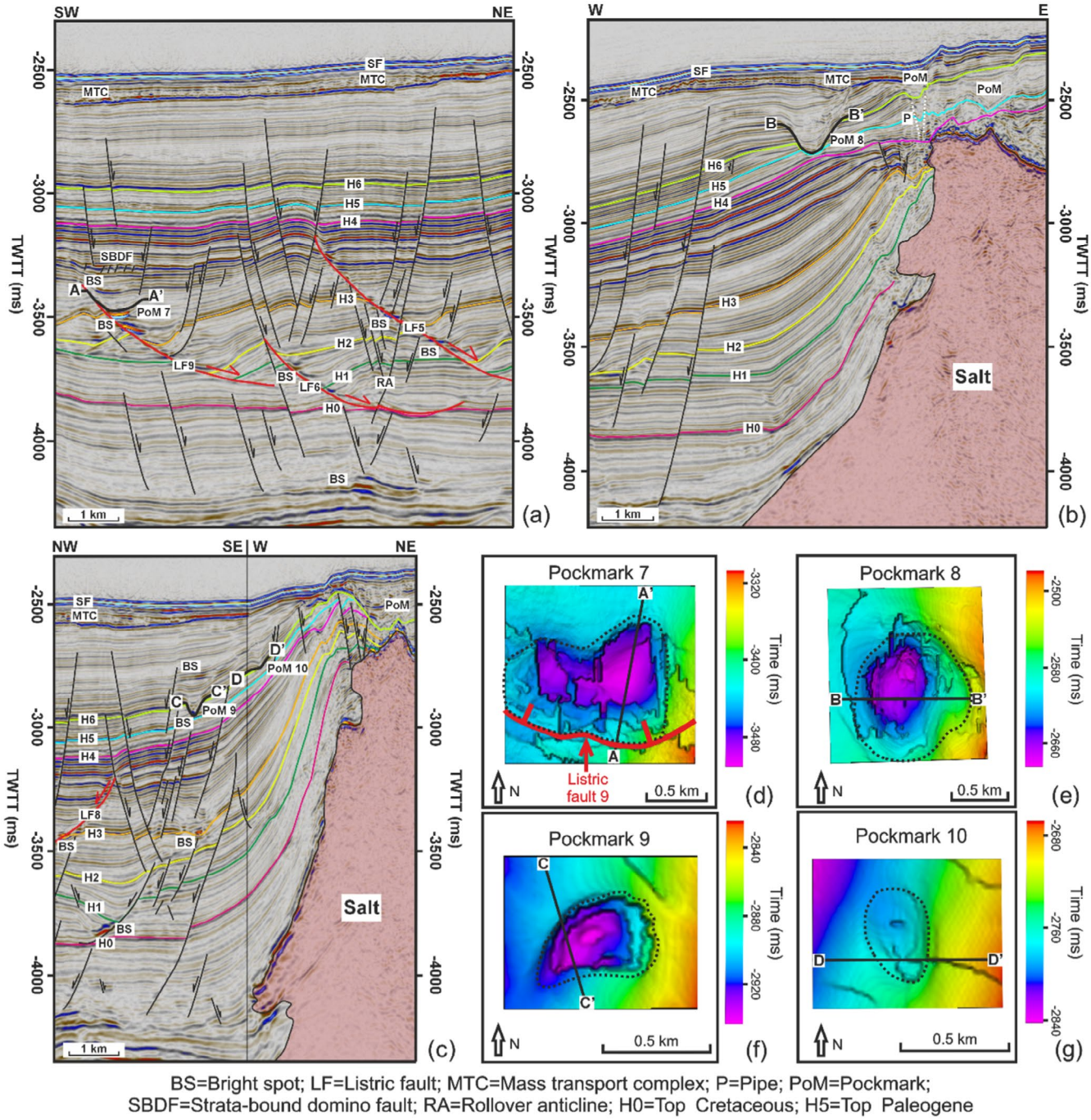

FIGURE 10 | Seismic profiles and TWTT structural maps highlighting the geometry and spatial distribution of pockmarks 7, 8, 9 and 10. (a–c) Seismic profiles across pockmarks interpreted in this work. (d–g) 3D visualisation of interpreted pockmarks, which are bounded by black dash polygons and adjacent listric faults. The black lines shown in (d–g) denote the seismic reflection in (a–c) marked by bold black lines. The location of seismic profiles and pockmarks is shown in Figures 5 and 7. Uninterpreted seismic profiles are also shown in Supporting Information File S1.

with these acting as fluid conduits. In contrast, fault hanging-wall pockmarks are developed away from the faults' traces, on their immediate hanging-wall blocks. Hence, pockmarks 2, 4 and 7 are fault-strike pockmarks, whereas pockmarks 1 and 3 are fault hanging-wall pockmarks (Figures 8–10). Fault-strike pockmarks (pockmarks 2, 4 and 7) are 1288 to 2283 m long,

739 to 1150 m wide and 75 to 139 m deep (Figures 8a,d and 10a; Table 2). In comparison, fault hanging-wall pockmarks (pockmarks 1 and 3) are 1674 to 2339 m long, 551 and 1177 m wide and 33 and 61 m deep (Figure 8a; Table 1). It is worth noting that pockmark 6 is a composite one, i.e. it is formed by multiple small pockmarks of the fault-strike and fault hanging-wall types (Figure 9).

Fault-strike pockmarks are deeper than fault hanging-wall pockmarks, though their length and width are similar. Moreover, fault-strike pockmarks show steeper internal slopes when compared to fault hanging-wall pockmarks (Table 1). This is because fault-strike pockmarks are bounded by the upper tips of listric faults, which are relatively steep. Additionally, fault-strike and fault hanging-wall pockmarks can develop as stacked pockmarks around the same listric fault, as demonstrated along listric fault 2 by the presence of pockmarks 2 and 3 (Figure 8a). This character suggests there were at least two periods of focused fluid seepage associated with listric fault 2, justifying the presence of stacked pockmarks around it.

Vertical fluid pipes are observed below Type I pockmarks, particular below fault-hanging pockmarks (Figures 8a and 9a–d). These pipes highlight the fluid flow pathways responsible for their formation (Cartwright 2007; Loseth et al. 2011; Cartwright and Santamarina 2015; Maestrelli et al. 2017). They are characterised by their low-amplitude, chaotic internal reflections with typical concave-upwards drag folds. In places, bright spots and other high-amplitude anomalies are also observed (Figure 9a–e). The boundary between pipes and surrounding strata is marked by the abrupt downward bending and dimming of seismic reflections, and seldom as clear offsets in seismic data (Figures 8a and 9a–9d).

Fluid pipes follow the orientation of overlying pockmarks and reveal elliptical or elongated shapes in plan view. They gradually widen upwards near the base of the pockmarks, recording a height of up to 200 ms (around 225 m). Fluid pipes terminate downwards in low-amplitude chaotic reflections around listric faults, and even on their planes (Figures 8a and 9). Moreover, bright spots are found below these fluid escape pipes in strata offset by listric faults, implying that fluids migrating upwards from these faults generated the pockmarks on the seafloor. Bright spots around listric faults and their surrounding strata are negative high-amplitude anomalies (Figures 6, 8a and 9a–d), likely due to the presence of gas. This gas can induce negative impedance contrasts in strata and dim their internal reflections (Cox, Newton, and Huuse 2020).

4.1.2 | Type II Pockmarks

Type II pockmarks are circular or elliptical in plan view, 426 to 1125 m long, 228 to 1061 m wide, and 23 to 138 m deep (Figures 8 and 10; Table 1). Their steep internal slopes of Type II pockmarks vary between 9° and 23°, while gentler internal slopes reach 8° to 20°. Type II pockmarks occupy an area between 0.1 to 0.9 km^2 and are found either in the hanging-wall of crestal faults or along the flanks of a salt wall (Figures 7, 8 and 10). Similarly to Type I, these Type II pockmarks occur above horizons H5 and H6, indicating that they were formed after the Paleogene. They are V-shaped in cross section and reveal onlapping fills (Figures 8d and 10a–c). Infilling sediment has low amplitude and is often chaotic (Figures 8d and 10b,c). The flank of the salt wall shows no fluid pipes below the pockmarks (Figures 8d and 9). As a result, it is hard to understand what fluid migration paths were responsible for the pockmarks. However, fluid escape pipes occur below these latter in the hanging-wall of crestal faults (Figure 10b,c).

Pockmarks 8, 9 and 10 were formed along the flank of a salt wall, while pockmark 5 occurs on the hanging-wall of crestal faults. A fluid pipe that is 461 ms (around 504 m) tall is found below pockmark 5 (Figure 8d). This pipe shows low- to middle-amplitude reflections with concave-upward reflections and brightened strata in its lower part. Internal reflections have much lower amplitude than surrounding strata, clearly defining its boundary. Furthermore, the pipe terminates downwards into a distinct bright spot that is preserved on the footwall of a crestal fault (Figure 8d), implying that the pipe is likely sourced from the unit offset by this fault. Such bright spots are of negative polarity, meaning that the migrating fluid is mainly gas. The presence of pockmark 5 near horizon H6 thus suggests the episodic eruption of gas around crestal faults.

4.2 | Geometry, Spatial Distribution, and Fluid-Flow Potential of Listric Faults

Listric faults are curved in plan view, striking NW-SE and WNW-ESE (Figure 7). They are 1019 to 7211 m long, dipping 1° to 26°, and showing maximum displacements of 386 to 1658 m. They dip to the NE and NNE, and sole out at depth (Figures 8–10). The interpreted listric faults occur in a salt minibasin and are deeper in the south when compared to their counterparts to the north. Most listric faults in the study area are also growth faults offset by surrounding crestal and keystone faults (see Zhang, Alves, and Martins-Ferreira 2022), suggesting that listric faults were formed relatively early (Figures 8–10). Crestal faults are of the radial and concentric types and were developed above salt structures, while keystone faults were formed in the lower parts of the salt minibasin as antithetic arrays delimiting symmetric extensional grabens (Figures 8–10). Rollover anticlines are also observed on the hanging-wall of listric faults 1, 2, 6 and 8 (Figures 8a and 9b–d). A buckle fold occurs in the lower part of listric fault 1 (Figure 8a), indicating the presence of compressive deformation resulting from the horizontal movement (heave) of the latter structure. Several bright spots are observed in strata offset by listric faults (Figures 8–10), meaning that fluids migrated through them.

Interpreted listric faults grew as isolated structures, except for listric fault 8, though some listric faults present rugged curves in their D_{max}-L plots that resemble the profiles of coherent fault families (Figure 11). These rugged profiles occur because listric faults were offset by younger (salt-related) faults, resulting in spurious displacement variations. It is worth noting that listric fault 2 extends beyond the limit of the seismic volume, and its D_{max}-L curve is truncated (Figures 7 and 11b). The formation of these listric faults has been discussed by Zhang, Alves, and

TABLE 2 | Attributes of listric faults interpreted in the study area.

Name	Strike	Dip	Length (m)	Maximum displacement (m)	Heave (m)	Throw (m)	Area (km^2)	Leakage factor	Average leakage factor	Relationship with seismic horizons
Listric fault 1	308°	3°–15°	3236	1248	1243	106	12.2	2.6–13.3	4.6	Offset H3-H6, detach in H2
Listric fault 2	324°	2°–13°	3700	736	736	25	5.6	3.1–11.5	4.8	Offset H4-H6, detach in H3
Listric fault 3	290°	7°–24°	2257	559	554	73	2.9	1.8–6.1	2.6	Offset H1-H2, detach in H0
Listric fault 4	314°	1°–12°	2342	716	715	25	6.1	3.6–10.0	4.9	Offset H3-H6, detach in H2
Listric fault 5	297°	6°–19°	4900	1300	1294	113	17.9	2.0–13.0	3.3	Offset H1-H3, detach in H0
Listric fault 6	301°	6°–23°	2152	1053	1043	146	2.5	2.0–4.2	2.7	Offset H1-H2, detach in H0
Listric fault 7	286°	7°–26°	1019	826	823	71	1.8	1.8–4.5	2.8	Offset H1-H2, detach in H0
Listric fault 8	281°	3°–13°	7211	1313	1313	33	26.1	0–21.3	5.7	Offset H1-H6, detach in H0
Listric fault 9	311°	6°–23°	2717	1658	1645	211	7.3	2.0–11.8	3.4	Offset H1-H3, detach in H0
Listric fault 10	324°	7°–22°	1762	386	384	42	2.1	1.8–4.1	2.5	Below H1, detach in H0

Note: Heaves and throws were recorded along listric faults near the areas recording displacement maxima. The location of these listric faults is shown in Figures 7–10.

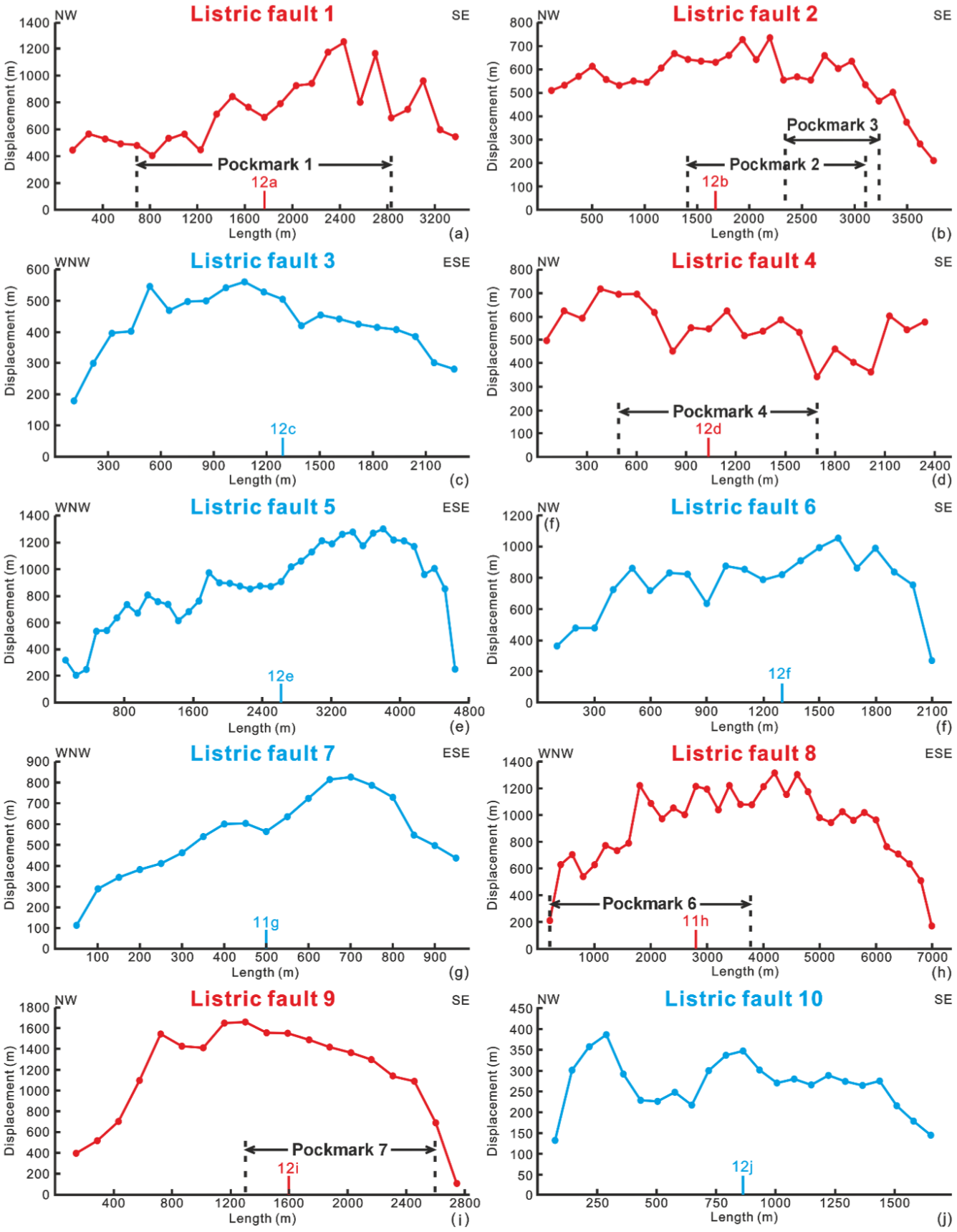

FIGURE 11 | Legend on next page.

FIGURE 11 | Displacement-length (D_{max}-L) plots along the ten listric faults interpreted in this work. LF1, LF2, LF4, LF8 and LF9 are listric faults with pockmarks and their length and displacement are usually larger than those listric faults without pockmarks, i.e. LF3, LF5, LF6, LF7 and LF10. Listric faults with pockmarks are shown as red lines, whereas listric faults without pockmarks are marked by blue lines. The position of pockmarks relative to their adjacent listric faults is indicated in the figure. The short vertical lines 12a—12j in D_{max}-L plots indicate the location of the D-Z plots in Figure 12.

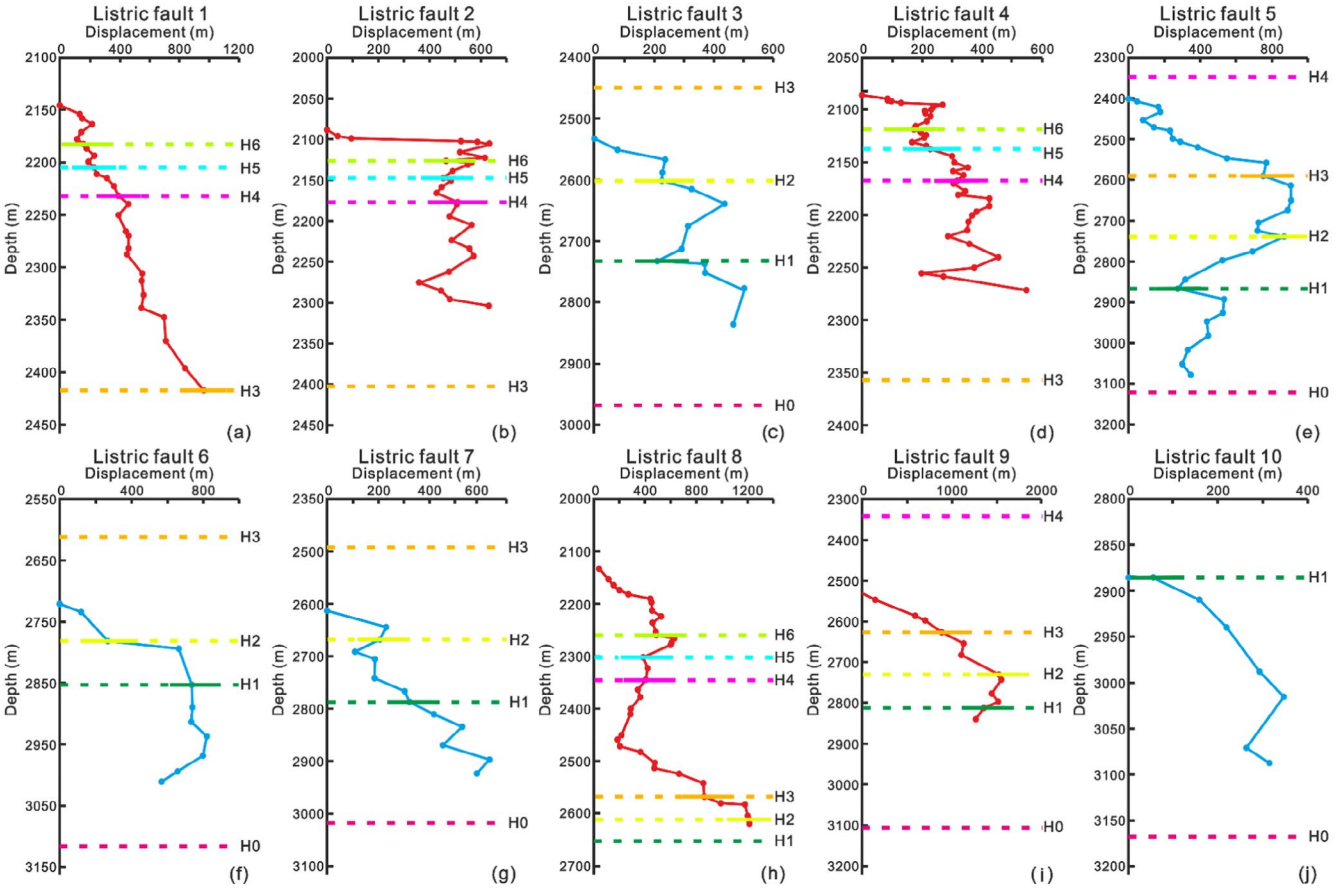

FIGURE 12 | Displacement–depth (D-Z) plots for the ten listric faults interpreted in this work. LF1, LF2, LF4, LF8 and LF9 are listric faults with pockmarks, and marked as red lines. In contrast, LF3, LF5, LF6, LF7 and L10 are buried below horizon 4 with no pockmarks. They are marked by blue lines in the figure. The location of these D-Z plots is shown by short vertical lines in Figure 11.

Martins-Ferreira (2022), which suggested it to be related to local overpressure build-up. Listric faults 1, 2 and 4 were formed in strata deposited between horizons H3 and H4, offsetting horizons H4 to H6 (Figure 8a,d). Listric fault 8 was formed by dip linkage, offsetting horizons H2 to H6 (Figure 9). Listric faults 3, 5, 6, 7, 9, and 10 were formed before horizon H4 (Figure 10a).

Five listric faults show pockmarks developed above them, or in their hanging-walls (Figures 8–10). Thus, we can classify listric faults into those with and without pockmarks. Listric faults with pockmarks includes faults 1, 2, 4, 8, and 9, whereas those without pockmarks include faults 3, 5, 6, 7, and 10 (Figures 8–10; Table 1). Listric faults with pockmarks show dips ranging from 1° to 23°, lengths ranging from 2342 to 7211 m, and a maximum displacement from 716 to 1658 m (Table 2). In comparison, listric faults without pockmarks dip 6° to 26°, are 1019 to 4900 m long, and show maximum displacements from 386 to 1300 m. Listric faults with pockmarks are usually broader, between 5.6 and 26.1 km^2 against 1.8–17.9 km^2 in faults without pockmarks. Interestingly, all listric faults with pockmarks offset horizons H4 to H6, except for listric fault 9. In contrast, listric faults without pockmarks occur below horizon H4 (Upper Eocene) at an average depth of 3020 ms (c. 2267 m) (Figures 8–10, 12 and 13). The relative depth of listric faults appears to be an important factor determining whether pockmarks are formed near listric faults.

Listric faults with pockmarks have relatively higher maximum and average leakage factors, revealing a greater probability of conducting fluids (Figure 14; Table 2). Listric faults with pockmarks record maximum leakage factors of 10.0 to 21.3, for an average value of 4.7. Listric faults without pockmarks have maximum leakage factors varying from 4.1 to 13.0, for an average value of 2.8. Importantly, listric faults record higher leakage factor values near their upper tips, when compared with their deeper parts, suggesting they are more likely to act as fluid migration paths. This agrees with the multiple bright spots

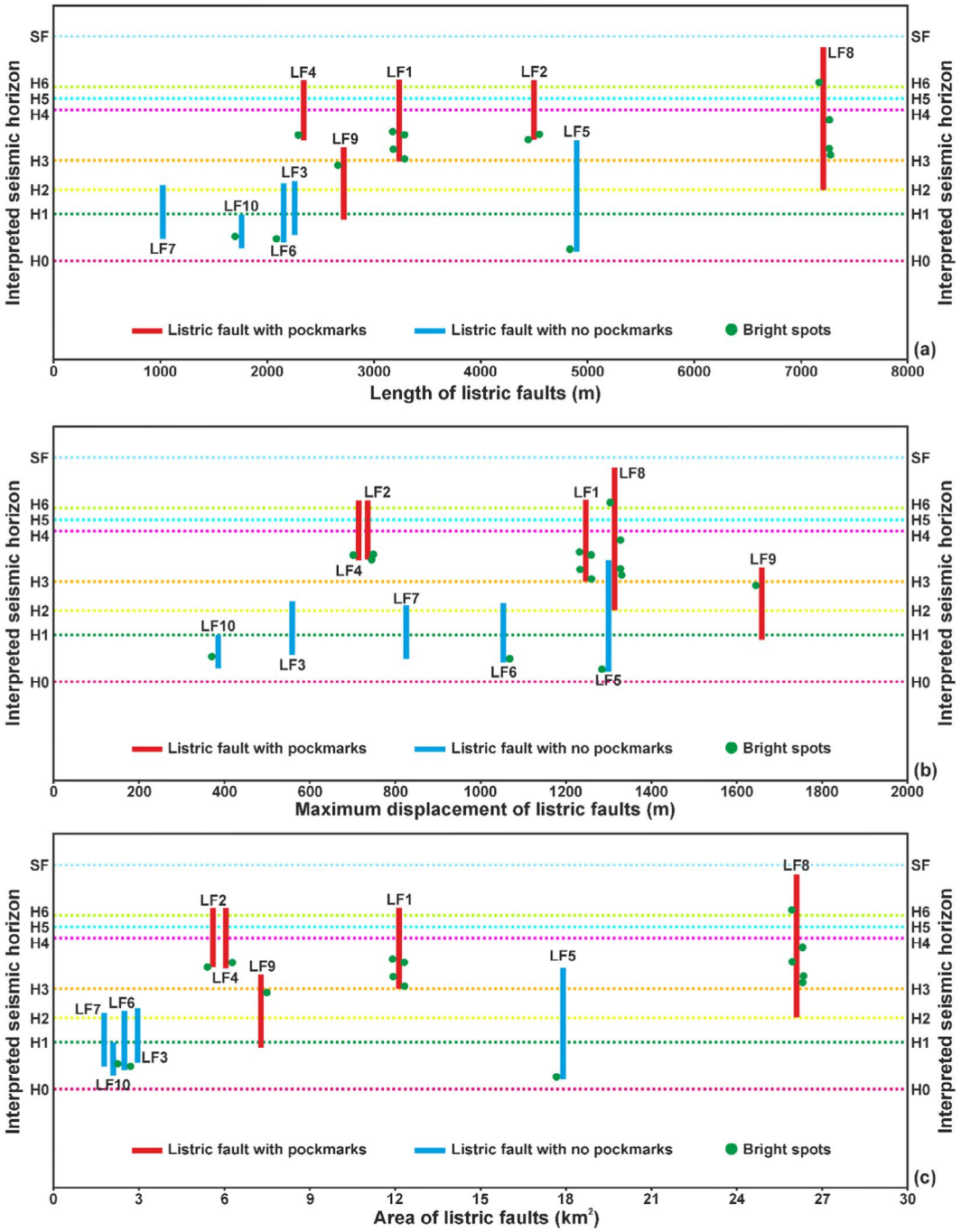

FIGURE 13 | Diagram illustrating the relationship between listric faults and pockmarks. (a) Length of listric faults; (b) Maximum displacement of listric faults; (c) Area of listric faults. The burial depth of each listric fault, relative to the interpreted horizons, is plotted based on the data in Figure 12. LF, Listric fault.

observed in the lower parts of listric faults, while Type I pockmarks are found around their upper tips (Figures 8–10).

5 | Discussion

5.1 | Relationship Between Buried Pockmarks and Adjacent Listric Faults

Several factors explain how listric faults control the formation of Type I pockmarks, including the relative depth, length, maximum displacement and area of the faults (Figure 13). As all listric faults without pockmarks occur below the Upper Paleogene horizon H4 (Figures 8–10, 12, and 13), there is a strong suggestion from our data that the depth of listric faults is a crucial factor determining whether pockmarks are formed. In other words, the deeper listric faults are subjected to higher overburden pressures and require the build-up of relatively high fluid overpressures to form any pockmarks. This is an interpretation that is consistent with our Leakage Factor analyses as the upper parts of listric faults, especially those listric faults with pockmarks, have a much higher probability of conducting fluids than their lower parts (Figure 14). The depth of listric faults is also associated with the timing of fluid migration and listric faults activity.

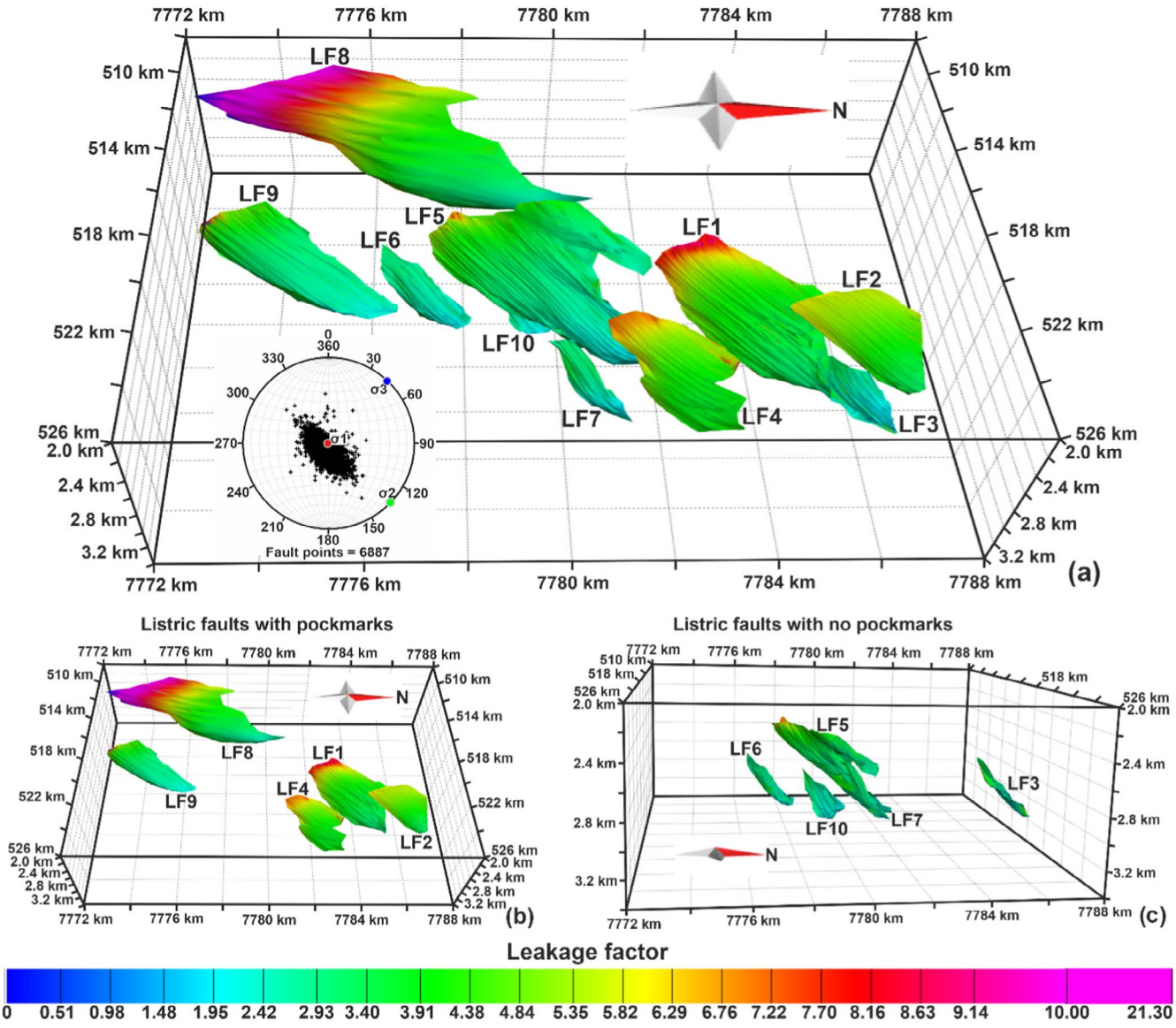

FIGURE 14 | (a) Leakage factor analysis for the ten interpreted listric faults using the palaeostress tensor obtained from stress inversion results in Zhang, Alves, and Martins-Ferreira (2022). The fault points obtained from ten interpreted listric faults are plotted as poles in the stereogram, revealing these listric faults dip to the NE with low angles. (b) and (c) Leakage factor analysis for listric faults with and without pockmarks. LF, Listric fault.

In the study area, focused fluid flow mainly occurred after the Paleogene; listric faults without pockmarks are only observed below horizon H4, and comprise Upper Eocene growth strata in adjacent hanging-wall depocentres (Figure 10a). Their growth ceased before the Miocene, so they did not act as favourable fluid flow pathways, the exception being listric fault 9—a structure buried below horizon H4 with a single pockmark 7 above it (Figure 10). Bright spots and strata-bounded domino faults are also observed around pockmark 7, hinting at local strata overpressure.

Listric faults with pockmarks are longer and broader than those without pockmarks, except for listric fault 5 identified below horizon H4 (Figure 13a,c). Hence, the length and area of listric faults may also be important factors controlling the formation of pockmarks. With increasing length and area, there is a greater chance for fluid to migrate through listric faults. As for faults' maximum displacement, it appears to control the formation of pockmarks such in the case of listric fault 9. However, no obvious differences occur when comparing the maximum displacements of listric faults with pockmarks against those without pockmarks (Figure 13b).

In order to quantify the relationship between pockmarks and their adjacent listric faults, we measured the displacement, vertical distance between listric faults and pockmarks, the dip of upper portion of listric faults, pockmark width, and pockmark depth in 79 profiles taken along the long axis of Type I pockmarks (Figure 15). Note that pockmark 6 is a composite feature consisting of multiple smaller pockmarks, so it is significantly wider than the other five pockmarks. This explains why pockmark 6 is considered an outlier in Figure 15b,d,f, and was discarded when generating the trendlines in these graphs. The data show that pockmark depth and width have a weak correlation with fault displacement, as their correlation coefficient values are merely 0.05 and 0.04 (Figure 15a,b). This

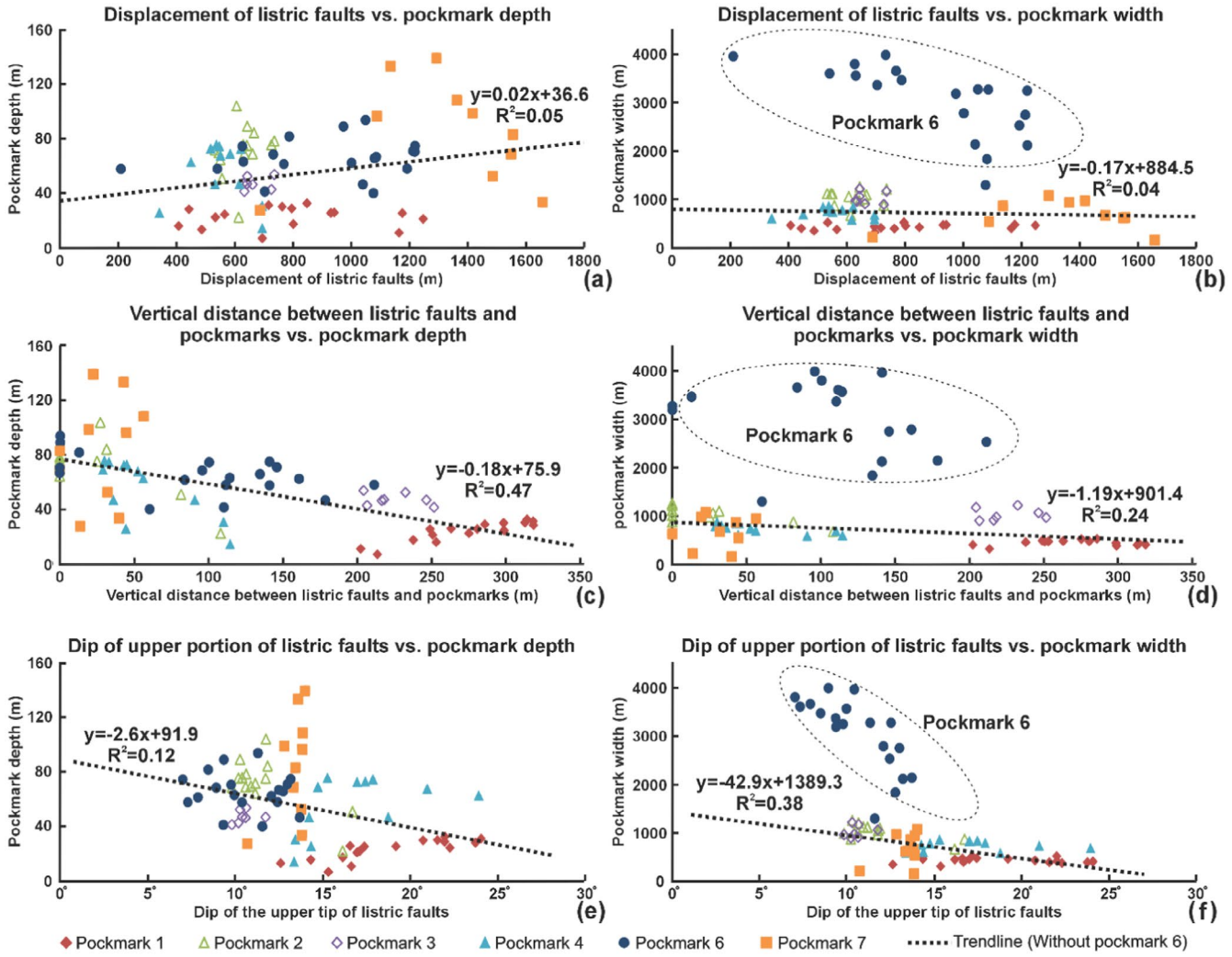

FIGURE 15 | Plots illustrating the relationship between pockmarks and adjacent listric faults. (a) Displacement of listric faults vs. pockmark depth; (b) Displacement of listric faults vs. pockmark width; (c) Vertical distance between listric faults and pockmarks vs. pockmark depth; (d) Vertical distance between listric faults and pockmarks vs. pockmark width; (e) Dip of the upper portion of listric faults vs. pockmark depth; (f) Dip of the upper portion of listric faults vs. pockmark width. Pockmark depth and width show a weak correlation with fault displacement, but a negative correlation with vertical distance between listric faults and pockmarks, and also with the dip of upper portion of listric faults. Note trendlines were generated without considering pockmark 6, which is a composite feature.

observation indicates that fault displacement had no effect on pockmark depth and width, though these pockmarks usually occur near the centre of listric faults, i.e. where relatively large displacements are recorded (Figure 11). Comparatively, pockmark depth and width show a negative correlation with the vertical distance between listric faults and the pockmarks themselves (Figure 15c,d). This suggests that fault-strike pockmarks are usually deeper than fault hanging-wall pockmarks, though they have similar lengths and widths. Such an observation is likely related to the continuing activity of listric growth faults, as the depth of fault-strike pockmarks can increase due hanging-wall subsidence during fault growth. Pockmark depth and width show a negative correlation with the dip of the upper portion of listric faults, but their correlation coefficient values are relatively low (Figure 15e,f). This justifies why listric faults with gentler upper portions show deeper and wider pockmarks above, a phenomenon likely related to the higher overpressures required to cause fluid escape from the gently dipping portion of listric faults when compared to their steepest parts.

5.2 | Formation of Buried Pockmarks in the Investigated Salt Minibasin

5.2.1 | Type I Pockmarks

Six (6) Type I pockmarks occur above five (5) interpreted listric faults, revealing that listric faults acted as conduits for migrating fluid, though they are more likely to be fluid barriers, or baffles, in their lower parts (Figure 14). According to Zhang, Alves, and Martins-Ferreira (2022), the intervals in which these listric faults sole out are potential source rocks that reached thermal maturity, due to a Eocene thermal episode recognised on well data. This thermal pulse correlates with the emplacement of the Abrolhos volcanic Plateau (Cobbold, Meisling,

and Mount 2001; Meisling, Cobbold, and Mount 2001; Gibbs, Brush, and Fiduk 2003; Fiduk et al. 2004; Maia et al. 2022). In addition, potential source rock intervals were deposited in Cretaceous intervals that overlie the Aptian salt unit, and this salt was capable of maturing any local source rocks due to their high thermal conductivity (Jensen 1983, 1990; Wilson and Ruppel 2007; Canova et al. 2018; Zhang and Alves 2024). Bright spots observed around listric faults are thus likely to be hydrocarbons, especially thermogenic gas, as the intervals into which listric faults sole out have generated hydrocarbons and resulting fluid overpressure within them. This is an interpretation that is also supported by presence of many bright spots around salt-related faults that propagated into the intervals detached by listric faults. Hydrocarbon migrating along listric faults is likely to be trapped in the deeper, lower angle parts of listric faults, while migrating towards the surface near their upper tips, thus forming bright spots and pockmarks in Miocene and younger strata. If the hydrocarbon escapes from the upper tip of a listric fault, it will form pockmarks along the strike of this fault regardless of their distance from the fault trace (Figure 16a), as documented by pockmarks 2, 4, and 7 (Figures 8a, 8b and 10a). In contrast, if hydrocarbons migrate out of a fault plane before reaching its upper tip, they will form pockmarks along the strike of the fault, but revealing a variable distance to the fault trace (Figure 16c), as shown by pockmarks 1 and 3 (Figure 8a). This phenomenon results in fluid migrating out of listric faults when the fluid overpressure exceeds overburden pressure, explaining the formation of fault hanging-wall pockmarks (Figure 16c).

The two processes above explain why Type I pockmarks formed at different stratigraphic levels, and different times. Hydrocarbon leakage from listric faults depends on the ratio between overpressure build-up around listric faults and the

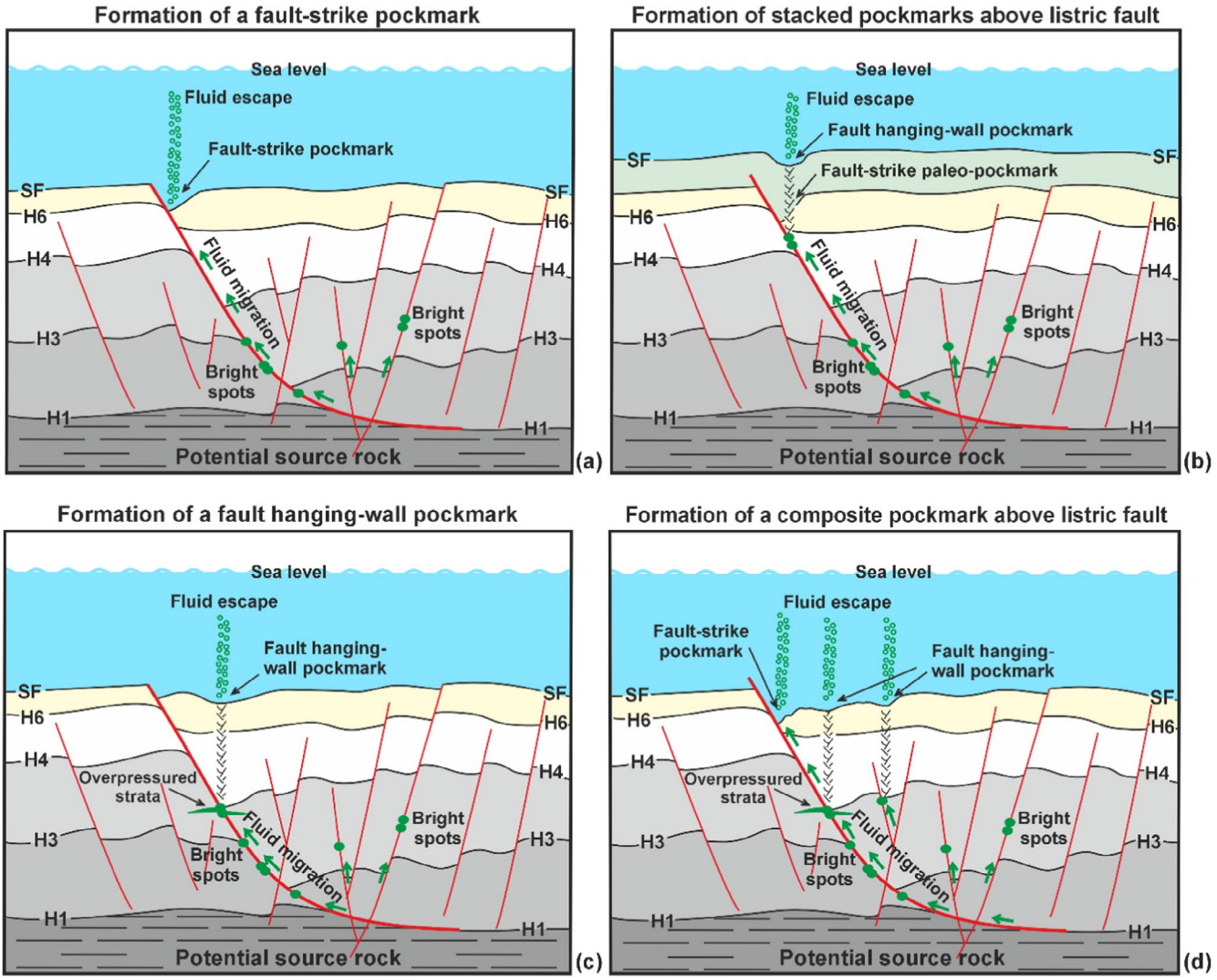

FIGURE 16 | Schematic illustrating the formation of pockmarks above a listric fault. (a) Hydrocarbon generated from a potential source rock migrates upwards along a listric fault and escapes from its upper tip, forming a fault-strike pockmark on the seafloor. (b) A new pockmark associated with hydrocarbon escape from a listric fault stacks above the previous pockmark, forming stacked pockmarks above a listric fault. (c) Hydrocarbon accumulates in faulted strata with the upwards migration of hydrocarbons along a listric fault, generating local overpressures in strata—this causes hydrocarbon migration from the listric fault when the overpressure is high enough to overcome overburden pressure. (d) Multiple pockmarks associated with hydrocarbon escape from a listric fault developed on its hanging-wall, generating a composite pockmark.

overburden pressure. The two processes can occur around listric faults at different times and locations. For example, pockmarks 2 and 3 are found above listric fault 2, where they appear as stacked in seismic data (Figure 8a). Pockmark 2 is a fault-strike pockmark, whereas pockmark 3 is a fault hanging-wall pockmark. Pockmark 2 was formed earlier than pockmark 3, and by a different process (Figure 16b). Another example is pockmark 6, a composite feature comprising multiple small pockmarks (Figure 9). These small pockmarks include fault-strike and fault hanging-wall pockmarks that were formed at a similar time above the same seismic reflection (Figure 16d).

5.2.2 | Type II Pockmarks

Type II pockmarks with circular or elliptical shapes were formed along the flank of a salt wall or near crestal faults (Figures 7, 8, and 10). Pockmark 5 is located around crestal faults that show a fluid escape pipe below, hinting at episodic fluid migration (Figure 8). This fluid escape pipe overlies a distinct bright spot observed on the footwall of a crestal fault. As this crestal fault offsets horizons H1-H3—delimiting potential source rocks—the fluids responsible for the formation of pockmark 5 are again likely to be hydrocarbons, especially thermogenic gas. Pockmarks 8, 9, and 10 were developed along the flank of salt wall (Figure 10), but are similar to those overlying its crest (Figure 10b,c). Pockmarks on the crest of this salt wall were documented in Tao and Alves (2023), who suggested they are formed due to salt seal failure. This type of pockmark has also been studied on the continental slope of the Santos Basin by de Mahiques et al. (2017); here, they form linear, network, concentric and radial pockmarks above large salt diapirs. De Mahiques et al. (2017) suggest that the formation of these pockmarks is associated with the development of underlying diapirs and their related faults, and speculated that these pockmarks extend further across the Campos and Espírito Santo Basins.

5.3 | Significance of Buried Pockmarks in Salt Minibasins

Although the six (6) Type I pockmarks were formed at different depths and times, most were developed above horizon H5—the Top Paleogene unconformity—after a major thermal pulse affecting the Espírito Santo Basin in the early to middle Eocene (Cobbold, Meisling, and Mount 2001; Meisling, Cobbold, and Mount 2001; Gibbs, Brush, and Fiduk 2003; Fiduk et al. 2004; Maia et al. 2022). Fluid migrating through Type I pockmarks was likely thermogenic gas produced from source rocks into which listric faults sole out. As for the other four Type II pockmarks, their formation is associated with fluid seeping from crestal faults or the salt structures per se due to salt seal failure. This implies that their generation accompanied the growth of underlying salt diapirs and related faults as documented by de Mahiques et al. (2017) and Tao and Alves (2023). Type II pockmarks are also developed above horizon H5, indicating that they post-date the Paleogene. In parallel, their formation partly correlates with the timing of the buried pockmark fields investigated by de Mahiques et al. (2017), and thus suggests that these pockmarks extend from the Campos and Santos Basins towards the Espírito Santo Basin. The study area is located near a region of anomalous heat flows where temperature gradients are higher than 30°C/km and the heat flow is in excess of 70 mW/m^2 (Hamza, Vieira, and Silva 2018), again implying that thermogenic fluids were likely generated from local source rocks. Moreover, leakage factor analyses show that listric faults, especially the upper parts of listric faults with pockmarks, have a higher probability to act as conduits for fluid (Figure 14). Therefore, they should be given particular attention in geohazard assessments offshore SE Brazil.

6 | Conclusions

This work aimed at understanding the geometry, distribution, formation, and significance of buried pockmarks and analysing its relationship with adjacent listric faults in a salt minibasin offshore Espírito Santo, SE Brazil. Main conclusions can be summarised as follows:

a. Six buried pockmarks associated with listric faults are interpreted based on seismic data and show crescent, elliptical or elongated shapes, with their long axes being near-parallel to the strike of their adjacent listric faults. These pockmarks are approximately 1300–6200 m long, 600–4000 m wide, and 30–139 m deep, and are buried between 50 and 500 m below the modern seafloor. They can be subdivided into fault-strike (Type I) and fault hanging-wall (Type II) pockmarks based on their spatial relationships.

b. The relative depth, length, area, and maximum displacement of listric faults are factors controlling whether pockmarks develop around them. Listric faults occurring below horizon H4—an Upper Paleogene unconformity—are unlikely to have pockmarks developed around them, as the timing of fluid flow in the study area occurred after the Paleogene. Listric faults with greater length, area, and maximum displacement were more likely to cause the formation of pockmarks. Moreover, pockmarks depth and width show a negative correlation with the dip of upper portions of listric faults, and also with the vertical distance between listric faults and pockmarks.

c. The formation of fault-strike and fault hanging-wall pockmarks is determined by two different fluid escape processes along listric faults. The fluids responsible for their formation are hydrocarbons, especially thermogenic gas, produced from the intervals into which listric faults sole out. Comparatively, pockmarks associated with crestal faults or salt structures are formed due to salt seal failure, and their formation also occurred after the Paleogene.

d. The presence of pockmarks associated with listric faults is clear evidence for local hydrocarbon escape occurring since the Miocene in the study area. Comparatively, the presence of pockmarks associated with crestal faults or salt structures reflects the growth of underlying salt diapirs and their related faults.

e. Listric faults, especially the upper parts of listric faults with pockmarks, have a higher probability to act as conduits for fluid leakage and should be given attention in future geohazard assessments offshore SE Brazil.

Acknowledgements

The authors acknowledge the permission conceded by CGG for the use of seismic data and the Brazilian National Petroleum Agency (ANP) for the well data provided. We thank Cerys Biancardi and Gwen Pettigrew for helping with our data interpretation and for managing software licences. The first author would like to acknowledge CSC (China Scholarship Council) for providing a PhD scholarship during his studies at Cardiff University. Schlumberger (providers of Petrel) and Petroleum Experts (Move) are acknowledged for the provision of the academic licences to Cardiff University 3D Seismic Lab. We are very grateful to Juan I. Soto, Clara Rodriguez and Qiliang Sun for their constructive reviews and comments on the manuscript.

Conflicts of Interest

The authors declare no conflicts of interest.

Data Availability Statement

The authors confirm that all relevant data are included in the paper. All additional data are available upon reasonable request to the authors.

References

Alves, T., M. Fetter, C. Busby, R. Gontijo, T. A. Cunha, and N. H. Mattos. 2020. "A Tectono-Stratigraphic Review of Continental Breakup on Intraplate Continental Margins and Its Impact on Resultant Hydrocarbon Systems." *Marine and Petroleum Geology* 117: 104341. https://doi.org/10.1016/j.marpetgeo.2020.104341.

Alves, T. M. 2012. "Scale-Relationships and Geometry of Normal Faults Reactivated During Gravitational Gliding of Albian Rafts (Espirito Santo Basin, SE Brazil)." *Earth and Planetary Science Letters* 331: 80–96. https://doi.org/10.1016/j.epsl.2012.03.014.

Alves, T. M., and T. Cunha. 2018. "A Phase of Transient Subsidence, Sediment Bypass and Deposition of Regressive–Transgressive Cycles During the Breakup of Iberia and Newfoundland." *Earth and Planetary Science Letters* 484: 168–183. https://doi.org/10.1016/j.epsl.2017.11.054.

Andresen, K. J., M. Huuse, and O. Clausen. 2008. "Morphology and Distribution of Oligocene and Miocene Pockmarks in the Danish North Sea–Implications for Bottom Current Activity and Fluid Migration." *Basin Research* 20, no. 3: 445–466. https://doi.org/10.1111/j.1365-2117.2008.00362.x.

Andresen, K. J., M. Huuse, N. H. Schødt, L. F. Clausen, and L. Seidler. 2011. "Hydrocarbon Plumbing Systems of Salt Minibasins Offshore Angola Revealed by Three-Dimensional Seismic Analysis." *AAPG Bulletin* 95, no. 6: 1039–1065. https://doi.org/10.1306/12131010046.

Barker, P., R. Buffler, and L. Gambôa. 1983. "A Seismic-Reflection Study of the Rio-Grande Rise." *Initial Reports of the Deep Sea Drilling Project* 72: 499–517. https://doi.org/10.2973/dsdp.proc.72.120.1983.

Betzler, C., S. Lindhorst, C. Hübscher, T. Lüdmann, J. Fürstenau, and J. Reijmer. 2011. "Giant Pockmarks in a Carbonate Platform (Maldives, Indian Ocean)." *Marine Geology* 289, no. 1–4: 1–16. https://doi.org/10.1016/j.margeo.2011.09.004.

Biancardi, C. A., T. M. Alves, and M. A. C. Martins-Ferreira. 2020. "Unpredictable Geometry and Depositional Stacking Patterns of Mass-Transport Complexes in Salt Minibasins." *Marine and Petroleum Geology* 120: 104522. https://doi.org/10.1016/j.marpetgeo.2020.104522.

Bruhn, C. H., and R. G. Walker. 1997. "Internal Architecture and Sedimentary Evolution of Coarse-Grained, Turbidite Channel-Levee Complexes, Early Eocene Regencia Canyon, Espirito Santo Basin, Brazil." *Sedimentology* 44, no. 1: 17–46. https://doi.org/10.1111/j.1365-3091.1997.tb00422.x.

Cainelli, C., and W. U. Mohriak. 1999. "Some Remarks on the Evolution of Sedimentary Basins Along the Eastern Brazilian Continental Margin." *Episodes* 22, no. 3: 206–216. https://doi.org/10.18814/epiiugs/1999/v22i3/008.

Canova, D. P., M. P. Fischer, R. S. Jayne, and R. M. Pollyea. 2018. "Advective Heat Transport and the Salt Chimney Effect: A Numerical Analysis." *Geofluids* 2018: 2378710. https://doi.org/10.1155/2018/2378710.

Cao, L., Q. Sun, and C. Magee. 2023. "Reutilization of Fluid Flow Pathways Over 54 Million Years, Offshore New Zealand." *Basin Research* 35: 2349–2363. https://doi.org/10.1111/bre.12801.

Cartwright, J. 2007. "The Impact of 3D Seismic Data on the Understanding of Compaction, Fluid Flow and Diagenesis in Sedimentary Basins." *Journal of the Geological Society* 164, no. 5: 881–893. https://doi.org/10.1144/0016-76492006-143.

Cartwright, J., M. Huuse, and A. Aplin. 2007. "Seal Bypass Systems." *AAPG Bulletin* 91, no. 8: 1141–1166. https://doi.org/10.1306/04090705181.

Cartwright, J., and C. Santamarina. 2015. "Seismic Characteristics of Fluid Escape Pipes in Sedimentary Basins: Implications for Pipe Genesis." *Marine and Petroleum Geology* 65: 126–140. https://doi.org/10.1016/j.marpetgeo.2015.03.023.

Cathles, L., Z. Su, and D. Chen. 2010. "The Physics of Gas Chimney and Pockmark Formation, With Implications for Assessment of Seafloor Hazards and Gas Sequestration." *Marine and Petroleum Geology* 27, no. 1: 82–91. https://doi.org/10.1016/j.marpetgeo.2009.09.010.

Chang, H. K., R. O. Kowsmann, A. M. F. Figueiredo, and A. A. Bender. 1992. "Tectonics and Stratigraphy of the East Brazil Rift System—An Overview." *Tectonophysics* 213, no. 1–2: 97–138. https://doi.org/10.1016/B978-0-444-89912-5.50032-6.

Chen, J., H. Song, Y. Guan, et al. 2015. "Morphologies, Classification and Genesis of Pockmarks, Mud Volcanoes and Associated Fluid Escape Features in the Northern Zhongjiannan Basin, South China Sea." *Deep Sea Research Part II: Topical Studies in Oceanography* 122: 106–117. https://doi.org/10.1016/j.dsr2.2015.11.007.

Cobbold, P. R., K. E. Meisling, and V. S. Mount. 2001. "Reactivation of an Obliquely Rifted Margin, Campos and Santos Basins, Southeastern Brazil." *AAPG Bulletin* 85, no. 11: 1925–1944. https://doi.org/10.1306/8626D0A9-173B-11D7-8645000102C1865D.

Cole, D., S. Stewart, and J. Cartwright. 2000. "Giant Irregular Pockmark Craters in the Palaeogene of the Outer Moray Firth Basin, UK North Sea." *Marine and Petroleum Geology* 17, no. 5: 563–577. https://doi.org/10.1016/s0264-8172(00)00013-1.

Cox, D. R., A. M. Newton, and M. Huuse. 2020. "Chapter 22- An Introduction to Seismic Reflection Data: Acquisition, Processing and Interpretation." In *Regional Geology and Tectonics*, edited by N. Scarselli, J. Adam, D. Chiarella, D. G. Roberts, and A. W. Bally, 571–603. Amsterdam: Elsevier. https://doi.org/10.1016/b978-0-444-64134-2.00020-1.

Davison, I. 2007. "Geology and Tectonics of the South Atlantic Brazilian Salt Basins." In *Deformation of the Continental Crust: The Legacy of Mike Coward*, edited by A. C. Ries, R. W. H. Butler, and R. H. Graham, vol. 272, 345–359. London: Geological Society of London. https://doi.org/10.1144/GSL.SP.2007.272.01.18.

Davison, I., L. Anderson, and P. Nuttall. 2012. "Salt Deposition, Loading and Gravity Drainage in the Campos and Santos Salt Basins, Salt Tectonics, Sediments and Prospectivity." *Geological Society of London* 363: 159–174. https://doi.org/10.1144/SP363.8.

Davy, B., I. Pecher, R. Wood, L. Carter, and K. Gohl. 2010. "Gas Escape Features Off New Zealand: Evidence of Massive Release of Methane From Hydrates." *Geophysical Research Letters* 37, no. 21: 1–5. https://doi.org/10.1029/2010gl045184.

de Mahiques, M. M., U. Schattner, M. Lazar, P. Y. G. Sumida, and L. A. P. de Souza. 2017. "An Extensive Pockmark Field on the Upper Atlantic Margin of Southeast Brazil: Spatial Analysis and Its Relationship With Salt Diapirism." *Heliyon* 3, no. 2: e00257. https://doi.org/10.1016/j.heliyon.2017.e00257.

Demercian, S., P. Szatmari, and P. Cobbold. 1993. "Style and Pattern of Salt Diapirs due to Thin-Skinned Gravitational Gliding, Campos and Santos Basins, Offshore Brazil." *Tectonophysics* 228, no. 3–4: 393–433. https://doi.org/10.1016/0040-1951(93)90351-J.

Dimitrov, L., and V. Dontcheva. 1994. "Seabed Pockmarks in the Southern Bulgarian Black Sea Zone." *Bulletin of the Geological Society of Denmark* 41: 24–33. https://doi.org/10.37570/bgsd-1995-41-02.

Ercilla, G. 1996. "Gas-Charged Sediments and Large Pockmark-Like Features on the Gulf of Cadiz Slope (SW Spain)." *Marine and Petroleum Geology* 13, no. 2: 253–261. https://doi.org/10.1016/0264-8172(95)00058-5.

Fader, G. B. 1991. "Gas-Related Sedimentary Features From the Eastern Canadian Continental Shelf." *Continental Shelf Research* 11, no. 8–10: 1123–1153. https://doi.org/10.1016/0278-4343(91)90094-m.

Fiduk, J. C., E. R. Brush, L. E. Anderson, P. B. Gibbs, and M. G. Rowan. 2004. "Salt Deformation, Magmatism, and Hydrocarbon Prospectivity in the Espirito Santo Basin, Offshore Brazil." In *Salt Sediment Interactions and Hydrocarbon Prospectivity Concepts, Applications and Case Studies for the 21st Century*, edited by P. J. Post, D. L. Olson, K. T. Lyons, S. L. Palmes, P. F. Harrison, and N. C. Rosen, vol. 24, Tulsa, OK: SEPM Society for Sedimentary Geology. https://doi.org/10.5724/gcs.04.24.0640.

Gamboa, D., T. Alves, J. Cartwright, and P. Terrinha. 2010. "MTD Distribution on a 'Passive' Continental Margin: The Espirito Santo Basin (SE Brazil) During the Palaeogene." *Marine and Petroleum Geology* 27, no. 7: 1311–1324. https://doi.org/10.1016/j.marpetgeo.2010.05.008.

Gamboa, D., T. M. Alves, and J. Cartwright. 2012. "A Submarine Channel Confluence Classification for Topographically Confined Slopes." *Marine and Petroleum Geology* 35, no. 1: 176–189. https://doi.org/10.1016/j.marpetgeo.2012.02.011.

Gamboa, D. A. 2011. *An Integrated Seismic-Scale Analysis of Reservoir Compartmentalisation on Continental Margins: The Espirito Santo Basin, SE Brazil, PhD*. Cardiff, UK: Cardiff University.

Gay, A., and C. Berndt. 2007. "Cessation/Reactivation of Polygonal Faulting and Effects on Fluid Flow in the Vøring Basin, Norwegian Margin." *Journal of the Geological Society* 164, no. 1: 129–141. https://doi.org/10.1144/0016-76492005-178.

Gay, A., M. Lopez, C. Berndt, and M. Séranne. 2007. "Geological Controls on Focused Fluid Flow Associated With Seafloor Seeps in the Lower Congo Basin." *Marine Geology* 244, no. 1–4: 68–92. https://doi.org/10.1016/j.margeo.2007.06.003.

Gay, A., M. Lopez, P. Cochonat, M. Séranne, D. Levaché, and G. Sermondadaz. 2006. "Isolated Seafloor Pockmarks Linked to BSRs, Fluid Chimneys, Polygonal Faults and Stacked Oligocene-Miocene Turbiditic Palaeochannels in the Lower Congo Basin." *Marine Geology* 226, no. 1–2: 25–40. https://doi.org/10.1016/j.margeo.2005.09.018.

Gay, A., M. Lopez, H. Ondreas, J. L. Charlou, G. Sermondadaz, and P. Cochonat. 2006. "Seafloor Facies Related to Upward Methane Flux Within a Giant Pockmark of the Lower Congo Basin." *Marine Geology* 226, no. 1–2: 81–95. https://doi.org/10.1016/j.margeo.2005.09.011.

Geldof, J.-B., J. Gafeira, J. Contet, and S. Marquet. 2014. "GIS Analysis of Pockmarks From 3D Seismic Exploration Surveys." https://doi.org/10.4043/25088-ms.In Proceedings Offshore Technology Conference.

Gibbs, P. B., E. R. Brush, and J. C. Fiduk. 2003. "The Evolution of the Syn Rift and Transition Phases of the Central/Southern Brazilian and W. African Conjugate Margins: The Implications for Source Rock Distribution in Time and Space, and Their Recognition on Seismic Data." https://doi.org/10.3997/2214-4609-pdb.168.arq_433.In Proceedings 8th International Congress of the Brazilian Geophysical Society.

Hamza, V. M., F. P. Vieira, and R. T. Silva. 2018. "Anomalous Heat Flow Belt Along the Continental Margin of Brazil." *International Journal of Earth Sciences* 107: 19–33. https://doi.org/10.1007/s00531-017-1503-8.

Hartwig, A., Z. Anka, and R. di Primio. 2012. "Evidence of a Widespread Paleo-Pockmarked Field in the Orange Basin: An Indication of an Early Eocene Massive Fluid Escape Event Offshore South Africa." *Marine Geology* 332: 222–234. https://doi.org/10.1016/j.margeo.2012.07.012.

Heggland, R. 1998. "Gas Seepage as an Indicator of Deeper Prospective Reservoirs. A Study Based on Exploration 3D Seismic Data." *Marine and Petroleum Geology* 15, no. 1: 1–9. https://doi.org/10.1016/s0264-8172(97)00060-3.

Hovland, M., J. V. Gardner, and A. Judd. 2002. "The Significance of Pockmarks to Understanding Fluid Flow Processes and Geohazards." *Geofluids* 2, no. 2: 127–136. https://doi.org/10.1046/j.1468-8123.2002.00028.x.

Hovland, M., R. Heggland, M. De Vries, and T. Tjelta. 2010. "Unit-Pockmarks and Their Potential Significance for Predicting Fluid Flow." *Marine and Petroleum Geology* 27, no. 6: 1190–1199. https://doi.org/10.1016/j.marpetgeo.2010.02.005.

Hovland, M., and A. G. Judd. 1988. *Seabed Pockmarks and Seepages: Impact on Geology, Biology and the Marine Environment*. London, UK: Graham & Trotman London.

Hovland, M., and J. H. Sommerville. 1985. "Characteristics of Two Natural Gas Seepages in the North Sea." *Marine and Petroleum Geology* 2, no. 4: 319–326. https://doi.org/10.1016/0264-8172(85)90027-3.

Hovland, M., H. Svensen, C. F. Forsberg, et al. 2005. "Complex Pockmarks With Carbonate-Ridges off Mid-Norway: Products of Sediment Degassing." *Marine Geology* 218, no. 1–4: 191–206. https://doi.org/10.1016/j.margeo.2005.04.005.

Jensen, P. K. 1983. "Calculations on the Thermal Conditions Around a Salt Diapir." *Geophysical Prospecting* 31, no. 3: 481–489. https://doi.org/10.1111/j.1365-2478.1983.tb01064.x.

Jensen, P. K. 1990. "Analysis of the Temperature Field Around Salt Diapirs." *Geothermics* 19, no. 3: 273–283. https://doi.org/10.1016/0375-6505(90)90047-F.

Judd, A., P. Croker, L. Tizzard, and C. Voisey. 2007. "Extensive Methane-Derived Authigenic Carbonates in the Irish Sea." *Geo-Marine Letters* 27: 259–267. https://doi.org/10.1007/s00367-007-0079-x.

Judd, A., and M. Hovland. 2007. *Seabed Fluid Flow: The Impact on Geology, Biology and the Marine Environment*. Cambridge, UK: Cambridge University Press.

King, L. H., and B. Maclean. 1970. "Pockmarks on the Scotian Shelf." *GSA Bulletin* 81, no. 10: 3141–3148. https://doi.org/10.1130/0016-7606(1970)81[3141:Potss]2.0.Co;2.

León, R., L. Somoza, T. Medialdea, et al. 2010. "Pockmarks, Collapses and Blind Valleys in the Gulf of Cádiz." *Geo-Marine Letters* 30: 231–247. https://doi.org/10.1007/s00367-009-0169-z.

Ligtenberg, H., and D. Connolly. 2003. "Chimney Detection and Interpretation, Revealing Sealing Qualityof Faults, Geohazards, Charge of and Leakage From Reservoirs." *Journal of Geochemical Exploration* 78: 385–387. https://doi.org/10.1016/s0375-6742(03)00095-5.

Loseth, H., L. Wensaas, B. Arntsen, N. M. Hanken, C. Basire, and K. Graue. 2011. "1000 m Long Gas Blow-Out Pipes." *Marine and Petroleum Geology* 28, no. 5: 1047–1060. https://doi.org/10.1016/j.marpetgeo.2010.10.001.

MacDonald, I. R., J. F. Reilly, N. L. Guinasso Jr., et al. 1990. "Chemosynthetic Mussels at a Brine-Filled Pockmark in the Northern

Gulf of Mexico." *Science* 248, no. 4959: 1096–1099. https://doi.org/10.1016/s0198-0254(06)80457-7.

Maestrelli, D., D. Iacopini, A. A. Jihad, C. E. Bond, and M. Bonini. 2017. "Seismic and Structural Characterization of Fluid Escape Pipes Using 3D and Partial Stack Seismic From the Loyal Field (Scotland, UK): A Multiphase and Repeated Intrusive Mechanism." *Marine and Petroleum Geology* 88: 489–510. https://doi.org/10.1016/j.marpetgeo.2017.08.016.

Maestro, A., A. Barnolas, L. Somoza, A. Lowrie, and T. Lawton. 2002. "Geometry and Structure Associated to Gas-Charged Sediments and Recent Growth Faults in the Ebro Delta (Spain)." *Marine Geology* 186, no. 3–4: 351–368. https://doi.org/10.1016/s0025-3227(02)00212-8.

Maia, T. M., A. C. dos Santos, S. C. Valente, et al. 2022. "Abrolhos Magmatic Province Petrogenesis and Its Link With the Vitória-Trindade Ridge, Southeast Brazilian Margin, South Atlantic Ocean." *Journal of South American Earth Sciences* 120: 104075. https://doi.org/10.1016/j.jsames.2022.104075.

Marcon, Y., H. Ondréas, H. Sahling, G. Bohrmann, and K. Olu. 2014. "Fluid Flow Regimes and Growth of a Giant Pockmark." *Geology* 42, no. 1: 63–66. https://doi.org/10.1130/g34801.1.

Masoumi, S., L. Reuning, S. Back, A. Sandrin, and P. A. Kukla. 2014. "Buried Pockmarks on the Top Chalk Surface of the Danish North Sea and Their Potential Significance for Interpreting Palaeocirculation Patterns." *International Journal of Earth Sciences* 103: 563–578. https://doi.org/10.1007/s00531-013-0977-2.

Mattos, N. H., and T. M. Alves. 2018. "Corridors of Crestal and Radial Faults Linking Salt Diapirs in the Espirito Santo Basin, SE Brazil." *Tectonophysics* 728: 55–74. https://doi.org/10.1016/j.tecto.2017.12.025.

Meisling, K. E., P. R. Cobbold, and V. S. Mount. 2001. "Segmentation of an Obliquely Rifted Margin, Campos and Santos Basins, Southeastern Brazil." *AAPG Bulletin* 85, no. 11: 1903–1924. https://doi.org/10.1306/8626d0a9-173b-11d7-8645000102c1865d.

Mitchum, R. M., Jr., P. R. Vail, and J. B. Sangree. 1977. *Seismic Stratigraphy and Global Changes of Sea Level: Part 6. Stratigraphic Interpretation of Seismic Reflection Patterns in Depositional Sequences: Section 2. Application of Seismic Reflection Configuration to Stratigraphic Interpretation, Seismic Stratigraphy—Applications to Hydrocarbon Exploration*. Vol. 26. Tulsa, OK: American Association of Petroleum Geologists. https://doi.org/10.1306/m26490c8.

Mohriak, W., M. Nemčok, and G. Enciso. 2008. "South Atlantic Divergent Margin Evolution: Rift-Border Uplift and Salt Tectonics in the Basins of SE Brazil, West Gondwana: Pre-Cenozoic Correlations Across the South Atlantic Region." *Geological Society of London* 294: 365–398. https://doi.org/10.1144/SP294.19.

Mohriak, W., and B. Rosendahl. 2003. "Transform zones in the South Atlantic rifted continental margins, Intraplate Strike-Slip Deformation Belts." *Geological Society of London* 210: 211–228. https://doi.org/10.1144/GSL.SP.2003.210.01.13.

Mohriak, W. U., P. Szatmari, and S. Anjos. 2012. "Salt: Geology and Tectonics of Selected Brazilian Basins in Their Global Context, Salt Tectonics, Sediments and Prospectivity." *Geological Society of London* 363: 131–158. https://doi.org/10.1144/SP363.7.

Ojeda, H. A. O. 1982. "Structural Framework, Stratigraphy, and Evolution of Brazilian Marginal Basins." *AAPG Bulletin* 66, no. 6: 732–749. https://doi.org/10.1306/03B5A309-16D1-11D7-8645000102C1865D.

Ondréas, H., K. Olu, Y. Fouquet, et al. 2005. "ROV Study of a Giant Pockmark on the Gabon Continental Margin." *Geo-Marine Letters* 25: 281–292. https://doi.org/10.1007/s00367-005-0213-6.

Piedade, A., and T. M. Alves. 2017. "Structural Styles of Albian Rafts in the Espirito Santo Basin (SE Brazil): Evidence for Late Raft Compartmentalisation on a 'Passive' Continental Margin." *Marine and Petroleum Geology* 79: 201–221. https://doi.org/10.1016/j.marpetgeo.2016.10.023.

Pilcher, R., and J. Argent. 2007. "Mega-Pockmarks and Linear Pockmark Trains on the West African Continental Margin." *Marine Geology* 244, no. 1: 15–32. https://doi.org/10.1016/j.margeo.2007.05.002.

Qin, Y. P., T. M. Alves, J. Constantine, and D. Gamboa. 2016. "Quantitative Seismic Geomorphology of a Submarine Channel System in SE Brazil (Espirito Santo Basin): Scale Comparison With Other Submarine Channel Systems." *Marine and Petroleum Geology* 78: 455–473. https://doi.org/10.1016/j.marpetgeo.2016.09.024.

Roelofse, C. 2020. *Fluid Flow Paths in Sedimentary Basins: Implications for Exploration in Challenging Geological Environments, PhD*. Cardiff, UK: Cardiff University.

Roelofse, C., T. M. Alves, and J. Gafeira. 2020. "Structural Controls on Shallow Fluid Flow and Associated Pockmark Fields in the East Breaks Area, Northern Gulf of Mexico." *Marine and Petroleum Geology* 112: 104074. https://doi.org/10.1016/j.marpetgeo.2019.104074.

Rouby, D., F. Guillocheau, C. Robin, et al. 2003. "Rates of Deformation of an Extensional Growth Fault/Raft System (Offshore Congo, West African Margin) From Combined Accommodation Measurements and 3-D Restoration." *Basin Research* 15, no. 2: 183–200. https://doi.org/10.1046/j.1365-2117.2003.00200.x.

Soter, S. 1999. "Macroscopic Seismic Anomalies and Submarine Pockmarks in the Corinth–Patras Rift, Greece." *Tectonophysics* 308, no. 1–2: 275–290. https://doi.org/10.1016/s0040-1951(99)00090-6.

Sun, Q., S. Wu, J. Cartwright, and D. Dong. 2012. "Shallow Gas and Focused Fluid Flow Systems in the Pearl River Mouth Basin, Northern South China Sea." *Marine Geology* 315–318: 1–14. https://doi.org/10.1016/j.margeo.2012.05.003.

Sun, Q., S. Wu, J. Cartwright, T. Lüdmann, and G. Yao. 2013. "Focused Fluid Flow Systems of the Zhongjiannan Basin and Guangle Uplift, South China Sea." *Basin Research* 25: 97–111. https://doi.org/10.1111/j.1365-2117.2012.00551.x.

Sun, Q., S. Wu, M. Hovland, P. Luo, Y. Lu, and T. Qu. 2011. "The Morphologies and Genesis of Mega-Pockmarks Near the Xisha Uplift, South China Sea." *Marine and Petroleum Geology* 28, no. 6: 1146–1156. https://doi.org/10.1016/j.marpetgeo.2011.03.003.

Tao, Z., and T. M. Alves. 2019. "Impacts of Data Sampling on the Interpretation of Normal Fault Propagation and Segment Linkage." *Tectonophysics* 762: 79–96. https://doi.org/10.1016/j.tecto.2019.03.013.

Tao, Z., and T. M. Alves. 2021. "Localized Strata-Bound Domino Faulting Offshore Espírito Santo Basin (Southeastern Brazil): The Case for Sudden Release of Fluid in Salt-Withdrawal Basins." *AAPG Bulletin* 105, no. 8: 1535–1562. https://doi.org/10.1306/01282117266.

Tao, Z., and T. M. Alves. 2023. "Seal Failure and Fluid Flow in Salt-Bearing Sedimentary Basins: A Critical Example From the Espírito Santo Basin, SE Brazil." *Marine and Petroleum Geology* 156: 106460. https://doi.org/10.1016/j.marpetgeo.2023.106460.

Velayatham, T., S. P. Holford, and M. A. Bunch. 2018. "Ancient Fluid Flow Recorded by Remarkably Long, Buried Pockmark Trains Observed in 3D Seismic Data, Exmouth Plateau, Northern Carnarvon Basin." *Marine and Petroleum Geology* 95: 303–313. https://doi.org/10.1016/j.marpetgeo.2018.05.007.

Vendeville, B. C. 2005. "Salt Tectonics Driven by Sediment Progradation: Part I—Mechanics and Kinematics." *AAPG Bulletin* 89, no. 8: 1071–1079. https://doi.org/10.1306/03310503063.

Wilson, A., and C. Ruppel. 2007. "Salt Tectonics and Shallow Subseafloor Fluid Convection: Models of Coupled Fluid-Heat-Salt Transport." *Geofluids* 7, no. 4: 377–386. https://doi.org/10.1111/j.1468-8123.2007.00191.x.

Zhang, Q., and T. Alves. 2024. "Contrasting Influence of Salt Structures and Faults on the Geothermal Potential of Regional Structural Highs: The Cleaver Bank High, Southern North Sea." *Geothermics* 116: 102842. https://doi.org/10.1016/j.geothermics.2023.102842.

Zhang, Q., T. M. Alves, and M. A. C. Martins-Ferreira. 2022. "Fault Analysis of a Salt Minibasin Offshore Espírito Santo, SE Brazil: Implications for Fluid Flow, Carbon and Energy Storage in Regions Dominated by Salt Tectonics." *Marine and Petroleum Geology* 143: 105805. https://doi.org/10.1016/j.marpetgeo.2022.105805.

Supporting Information

Additional supporting information can be found online in the Supporting Information section.